AWARD NUMBER: W81XWH-18-1-0263

TITLE: A Novel Combination Treatment for Ovarian Granulosa Cell Tumors

PRINCIPAL INVESTIGATOR: Dr Simon Chu

CONTRACTING ORGANIZATION: Hudson Institute of Medical Research
Clayton, Victoria, Australia

REPORT DATE: July 2019

TYPE OF REPORT: Annual Report

PREPARED FOR: U.S. Army Medical Research and Development Command
Fort Detrick, Maryland 21702-5012

REPORT DOCUMENTATION PAGE

Form Approved
OMB No. 0704-0188

PLEASE DO NOT RETURN YOUR FORM TO THE ABOVE ADDRESS.

1. REPORT DATE *(DD-MM-YYYY)*	2. REPORT TYPE	3. DATES COVERED *(From - To)*
July 2019	Annual Report	1JUL2018 - 30JUN2019

4. TITLE AND SUBTITLE

A Novel Combination Treatment for Ovarian Granulosa Cell Tumors

5a. CONTRACT NUMBER

5b. GRANT NUMBER

W81XWH-18-1-0263

5c. PROGRAM ELEMENT NUMBER

6. AUTHOR(S)

Dr Simon Chu

5d. PROJECT NUMBER

5e. TASK NUMBER

5f. WORK UNIT NUMBER

7. PERFORMING ORGANIZATION NAME(S) AND ADDRESS(ES)

Hudson Institute of Medical Research
27 - 31 Wright Street, Clayton, 3168, Victoria, Australia

8. PERFORMING ORGANIZATION REPORT NUMBER

9. SPONSORING/MONITORING AGENCY NAME(S) AND ADDRESS(ES)

U.S. Army Medical Research and Development Command (USAMRDC),
Fort Detrick, MD 21702-5012

10. SPONSOR/MONITOR'S ACRONYM(S)

11. SPONSOR/MONITOR'S REPORT NUMBER(S)

12. DISTRIBUTION/AVAILABILITY STATEMENT

Approved for Public Release; Distribution Unlimited

13. SUPPLEMENTARY NOTES

14. ABSTRACT

Ovarian granulosa cell tumors (GCT) are hormonally-active neoplasms characterized by endocrine manifestations, an indolent course and late recurrence. Treatment involves surgery, and chemo- or hormonal-therapy have limited efficacy. The hypothesis of this proposal is that 1) PPARgamma and XIAP play fundamental roles in the regulation of granulosa cell (GC) apoptosis, and/or terminal differentiation, albeit in a reciprocal manner, and 2) that combined targeting of PPARgamma and XIAP presents a novel therapeutic strategy for GCT treatment. Our specific aims are to 1) demonstrate the efficacy of PPARgamma activation in combination with XIAP inhibition for the treatment of GCT in a xenograft and 3D cell culture model; 2) elucidate the mechanisms of PPAR□induced apoptosis and/or differentiation through analysis of the PPARgammacistrome and transcriptome in GC- and GCT-derived cells; and 3) to determine the mechanistic consequences of XIAP inhibition and PPAR□activation at the proteomic level in GCT. We have evidence to show in vitro that the combination therapy proposed is efficacious in GCT-derived cell lines and in GCT tissue explants. An investigation of the genes that regulate this response indicate an activation of the NFkappaB

15. SUBJECT TERMS

Ovarian Cancer, Granulosa Cell Tumors, XIAP, PPARgamma, Smac-mimetics

16. SECURITY CLASSIFICATION OF:			17. LIMITATION OF ABSTRACT	18. NUMBER OF PAGES	19a. NAME OF RESPONSIBLE PERSON
a. REPORT	b. ABSTRACT	c. THIS PAGE			USAMRMC
U	U	U	UU	44	19b. TELEPHONE NUMBER *(Include area code)*

Reset

Standard Form 298 (Rev. 8/98)
Prescribed by ANSI Std. Z39.18

TABLE OF CONTENTS

	Page
1. Introduction	4
2. Keywords	4
3. Accomplishments	4 - 13
4. Impact	14 - 15
5. Changes/Problems	15 - 16
6. Products	16 - 18
7. Participants & Other Collaborating Organizations	18 - 20
8. Special Reporting Requirements	20
9. Appendices	20 - 44

1. INTRODUCTION:

Background: Ovarian granulosa cell tumors (GCT) are hormonally-active neoplasms characterized by endocrine manifestations, an indolent course and late recurrence. Treatment involves surgery, and chemo- or hormonal-therapy have limited efficacy. This proposal will address the development of a novel GCT-specific therapeutic strategy. The survival transcription factor, NFκB, is activated in these tumors; inhibition of this pathway promotes apoptosis. Peroxisome proliferator-activated receptor-gamma protein (PPARγ), a transcription factor that impedes growth and promotes differentiation, is overexpressed in GCT, but transrepressed by NFκB signalling in GCT. An NFκB-induced protein, X-linked inhibitor of apoptosis protein (XIAP), is also overexpressed in GCT and is critical in preventing GCT cell apoptosis and represents an attractive therapeutic target. We **hypothesize** that 1) PPARγ and XIAP play fundamental roles in the regulation of granulosa cell (GC) apoptosis, and/or terminal differentiation, albeit in a reciprocal manner, and 2) that combined targeting of PPARγ and XIAP presents a novel therapeutic strategy for GCT treatment.

2. KEYWORDS:

Ovarian Cancer; Granulosa Cell Tumors, X-Linked Inhibitor Of Apoptosis Proteins (XIAP); Peroxisome Proliferator Activated Protein (PPARγ)

3. ACCOMPLISHMENTS:

What were the major goals of the project?

Specific Aim 1(specified in proposal)	Timeline	Site 1	Status
Major Task 1: Demonstrate the efficacy of PPARγ activation in combination with XIAP inhibition for the treatment of GCT in a xenograft model.	Months		
Submission of institutional approved animal protocols and related material for DoD's ACURO approval	-2 to -3	SC	Expect approval in Nov 2020 – see Problems
Receive ACURO approval before initiating experiments	0 - 2	SC	
Submission of institution's IRB approval and related material for DoD's HRPO approval	-2 to -3	SC PJF	Approved
Receive HRPO approval before initiating experiments	0 – 2	SC PJF	

Subtask 1: Stable transfection of parental GCT-derived cells with RFP expression vector Appointment of research assistant and part time Postdoc for the *in vitro* studies	1-3	SC	Complete Nov 2018
Subtask 2: Establishment of parental and TET-on GCT-derived cell line xenografts	5-12	SC	Complete July 2019
Subtask 3: Breeding to generate between 100 to 120 NOD/SCID mice for xenograft and/or PDX experiments. Colonies of NOD/SCID mice are established at our Institute. For the xenograft studies we will require approximately 100 to 120 mice. In order to generate this number, we will maintain 6 pairs / year x 7 litters (n=6 pups / litter; 50% female).	5-16	SC	Postponed 2021
Subtask 4: Mice randomized and treated with the treatment regimen outlined in the proposal The *in vivo* animal model proposed in Aim 1.1 requires groups of 6 x nod/SCID mice for each experimental regimen (n=8) for each cell line. This equates to 6 mice x 8 (treatments) x 2 (cell lines) = 96 mice.	7-16	SC PJF JS	Postponed 2021
Subtask 5: xenografts removed for analysis (number, dimension, weight, volume and histology). Protein expression for markers of proliferation; apoptosis; angiogenesis; and the target proteins; XIAP and PPARγ will be examined using immunohistochemistry.	9 – 24	SC	Postponed 2021
Subtask 6: PDX models – dependent on availability of patient tissue from surgery – this will follow a similar regimen as outlined above for the xenograft models. Expected animal numbers: For every PDX sample, we expect to grow in 4 animals with 4 harvests over 3 years = 16 animals	7- 24	SC PJF JS	Postponed 2021
Major Task 2: Demonstrate the efficacy of PPARγ activation in combination with XIAP inhibition for the treatment of GCT in an ex-vivo and 3D cell culture model.			
Subtask 1: Spheroid experiments will commence with treatments	6 - 15	SC JS	Complete Jan 2019
Subtask 2: ex-vivo explant studies of patient material should they be collected during this period	6 - 36	SC PJF	Complete Jan 2019
Subtask 3: Manuscript prepared for xenograft and 3D model findings	24 -	SC PJF	3D Model Published 2019

Specific Aim 2 (specified in proposal)	Timeline	Site 1	Status
Major Task 3: To elucidate the mechanisms of PPARγ induced apoptosis and/or differentiation through analysis of the PPARγ cistrome in GC- and GCT-derived cells.			
Subtask 1: Treatment of cell lines will begin, and chromatin prepared for ChIP-Seq (Aim 2.1).	1 - 6	SC	Complete March 2020
Subtask 2: Perform ChIP-Seq			Samples to be submitted Nov 2020
Subtask 3: ChIP-Seq Bioinformatic analysis using specific pipelines outlined (Aim 2.1). Differentially expressed genes will be identified and the best candidates chosen for characterization (Aim 2.3).	12 - 18	SC RF	To be performed 2021
Major Task 4: To elucidate the mechanisms of PPARγ induced apoptosis and/or differentiation through analysis of the PPARγ transcriptome in GC- and GCT-derived cells.			
Subtask 1: Treatment of cell lines and RNA prepared for RNA-Seq (Aim 2.2).	6-12	SC RF	Completed October 2020
Subtask 2: Perform RNA-Seq	1-6	SC	Samples submitted October 2020
Subtask 3: RNA-Seq Bioinformatic analysis using specific pipelines outlined (Aim 2.2). Differentially expressed genes will be identified and the best candidates chosen for characterization (Aim 2.3).	6-9	SC	Results received Mar 2020 – in progress
Major Task 5: Determining the functional significance of PPARγ-regulated genes			
Subtask 1: Submission of ethics proposals to institutional animal ethics committee	12 – 13	SC	Submission Nov 2020
Subtask 2: Submission of institutional approved animal protocols and related material for DoD's ACURO approval	14 – 15	SC	
Subtask 3: Receive ACURO approval before initiating experiments	16 - 17	SC	
Subtask 4: Characterization of PPARγ-regulated genes will commence (Aim 2.3 (a), (b) and (c)).	18-24	SC RF PJF	In Progress
Subtask 5: Knockdown or re-expressed expression in cells (Aim 2.3c).	24 - 30	SC	In Progress

Subtask 6: Assessment for proliferation, viability, apoptosis, invasiveness, transactivation assays, colony formation assays and xenografts in gene knock down or re-expression in GC- and GCT-derived cell lines. Estimated animal numbers for xenograft experiments: groups of 6 x nod/SCID mice for each cell line with either knock-down or overexpression of candidate genes identified (n=5),for each cell line ie 6 mice x 5 (candidates) x 2 (cell lines) = 60 mice.	26 - 36	SC PJF	In Progress
Subtask 7: Publication preparation for Aim 2	30 - 36	SC RF JS PJF	Aim to submit July 2021
Major Task 6: To determine the mechanistic consequences of XIAP inhibition and PPARγ activation at the proteomic level in GCT.			
Subtask 1: Transduction experiments will begin with wild type and mutant XIAP expression vectors re-expressed (n=5 expression constructs) in XIAP-deficient cell lines (Aim 3.1).	1 - 6	SC	Complete March 2019
Subtask 2: SILAC experiments commenced using cell lines with XIAP re-expression (Aim 3.1).	6-18	SC JS AS	In Progress
Subtask 3: Aim 3.1 will have been completed. Bioinformatic analysis completed. Aim 3.2 characterization of top 2 candidate proteins will have commenced.	12 - 24	SC JS AS	In Progress
Subtask 4: Integration of SILAC data, ChIP-Seq data and RNA-Seq data will be performed.	24 - 36	SC RF AS JS PJF	In Progress
Subtask 5: Publication of Aim 2 and 3 findings completed	36	SC RF JS AS PJF	Aim to submit Dec 2021

What was accomplished under these goals?

Specific Aims: 1. To demonstrate the efficacy of PPARγ activation in combination with XIAP inhibition for the treatment of GCT in a xenograft and 3D cell culture model; **2.** To elucidate the mechanisms of PPARγ induced apoptosis and/or differentiation through analysis of the PPARγ cistrome and transcriptome in GC- and GCT-derived cells; and **3.** To determine the mechanistic consequences of XIAP inhibition and PPARγ activation at the proteomic level in GCT.

Update on Progress:

Aim 1. To demonstrate the efficacy of PPARγ activation in combination with XIAP inhibition for the treatment of GCT in a xenograft and 3D cell culture model.

Rationale

Targeting more than one pathway in cancer is known to be more efficacious than targeting a single pathway (Fulda and Vucic 2012). Building on our *in vitro* findings using monolayer cultures, we will show that PPARγ activation and XIAP inhibition abrogates tumor development using: (i) an *in vivo* murine xenograft preclinical model; and (ii) an *ex vivo* explant and an established 3D cell culture model that mimics the tumor microenvironment.

Results:

Aim 1.2: Develop *ex vivo* explant and 3D cell culture models

We have previously described *PPARγ* mRNA overexpression in GCT (n=12) and the GCT-derived cell lines (KGN and COV434) (Alexiadis M et al 2011). Using quantitative RT-PCR, we observed that *XIAP* was abundantly expressed in the cell lines and was significantly upregulated in GCT compared with whole normal ovary samples (**Figure 1A**). *XIAP* mRNA expression did not differ between stage 1 and advanced stage GCT. The expression of XIAP and PPARγ was also examined at the protein level using IHC, which demonstrated strong staining for both proteins (**Figure 1B**). Tissue microarray analysis (TMA) revealed that XIAP expression was high in 52/76 (68%) of the primary tumor samples (**Figure 1C** and **Table 1**). For those tumor samples with both primary and recurrent cores, we observed that XIAP expression did not differ between tumor samples (**Table 1**). XIAP expression was observed in the granulosa cells of both small follicles and a preovulatory follicle, as well as in the surrounding theca in a normal preovulatory ovarian sample (**Figure 1C**).

We observed very low expression of cIAP1 in all tissues examined (**Figure 1C**), while no expression of cIAP2 was observed.

Consistent with our previous observation of high *PPARγ* mRNA levels, we observed high levels with IHC for PPARγ in the majority of the GCT cores in the TMA. Moderate to high expression of PPARγ was observed for 49/76 (64%) of primary GCT (**Figure 1C** and **Table 1**), with only 1 tumor showing less expression in a recurrent tumor compared to the primary tumor (data not shown). Nuclear staining was observed in the granulosa cells of the small and preovulatory follicle in the normal preovulatory ovarian sample (**Figure 1C**), while both nuclear and cytoplasmic staining was observed in the cells of the surrounding stroma.

Figure 1

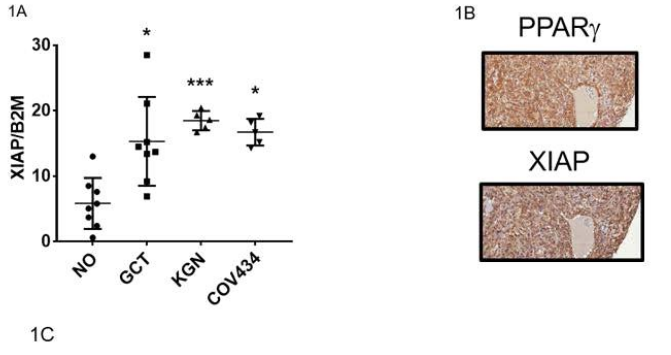

Table 1. XIAP and PPARγ protein expression on GCT tissue microarray[a]

	GCT tissue microarray (n = 76: 52 primary tumors only; 4 recurrent tumors only)[b]	
	Low	Medium/high
Marker	*n* (%)	*n* (%)
XIAP	24 (32)	52 (68)
PPARγ	27 (36)	49 (64)

[a]Staining was analyzed using "positive pixel count v9" algorithm in the Aperio ImageScope version 12.3.0.5056 (Leica Biosystems). Percentage of positive (brown) staining indicating protein levels was determined as low (0%–30%), medium (31%–79%), or high (>80%).

[b]Each sample represents a GCT collected from an individual patient. Of the 52 primary tumors, 20 have multiple samples and 4 patients have developed recurrent diseases, which were included in the cohort. The tumor samples with both primary and recurrent cores were scored medium/high for XIAP and PPARγ expression.

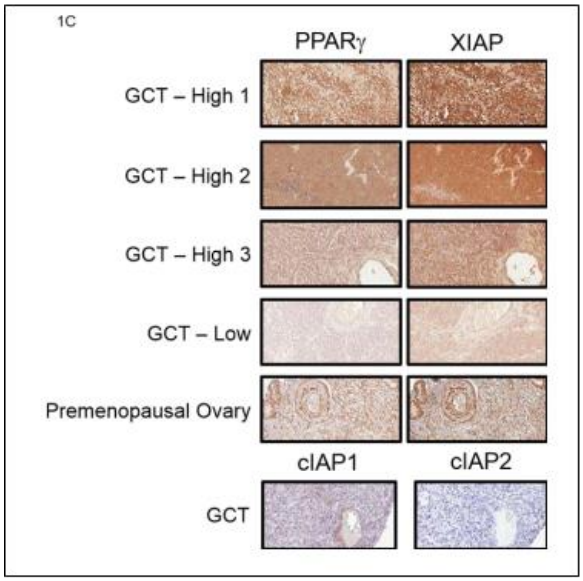

Inhibiting XIAP decreases NFκB and AP1 transactivation preventing NFκB transrepression and potently sensitizing KGN and COV434 cells to PPARγ-mediated apoptosis.

We determined if inhibiting XIAP could also decrease the constitutive activity of NFκB and AP1 in the GCT-derived cell lines. When cells were transfected with either a NFκB or AP1 reporter, there was an approximate 6-fold induction of luciferase activity under basal conditions compared with cells transfected with an enhancer-less reporter (pTAL-Luc; **Fig. 2A and B**). Treating KGN cells with 5 mmol/L BAY11-7082 or 20 mmol/L PD-98059 (PD; ERK/AP1 inhibitor) suppressed the respective constitutive activity. When we treated KGN cells with a Smac-mimetic, CmpdA (500 nmol/L), the constitutive activity was abrogated for both pathways. A similar result was observed for the COV434 cell line (data not shown).

As inhibition of XIAP abrogates the constitutive activity of both the NFκB and AP1 signaling pathways, we hypothesized that inhibition of XIAP would remove NFkB-mediated transrepression of PPARγ. Using the xCELLigence RTCA system to assess cell proliferation in real time, we assessed the effect of CmpdA (500 nmol/L) either as a single treatment, or in combination with the PPARγ agonists KGN and COV434 cells, and in a nonluteinized granulosa cell line, hGrC1. When cells were treated with CmpdA alone, there was no effect on cell proliferation for either the GCT-derived cell lines (**Fig. 2C and D**) or the hGrC1 cells (**Fig. 2E**) over 72 hours. In addition, CmpdA alone also had no effect on PPARg transactivation (**Fig. 2F**) or apoptosis (**Fig. 2G and H**). PPARγ activation alone with RGZ/RA or TGZ/RA caused a small decrease in proliferation (**Fig. 2C–E**) with no effect on apoptosis (**Fig. 2G and H**). Combining CmpdA and with RGZ/RA (20 mmol/L/5 mmol/L) resulted in cessation of cell proliferation in both KGN (**Fig. 2C**) and COV434 (**Fig. 2D**) cells over 72 hours. This was accompanied by robust PPARγ-mediated transactivation of the reporter construct (**Fig. 2F**) and significant increase in apoptosis (**Fig. 2G and H**). Consistent results were observed when a monomeric Smac-mimetic AZD5582 was used in combination with RGZ/RA or with another PPARγ agonist, TGZ (Data not shown).

Figure 2

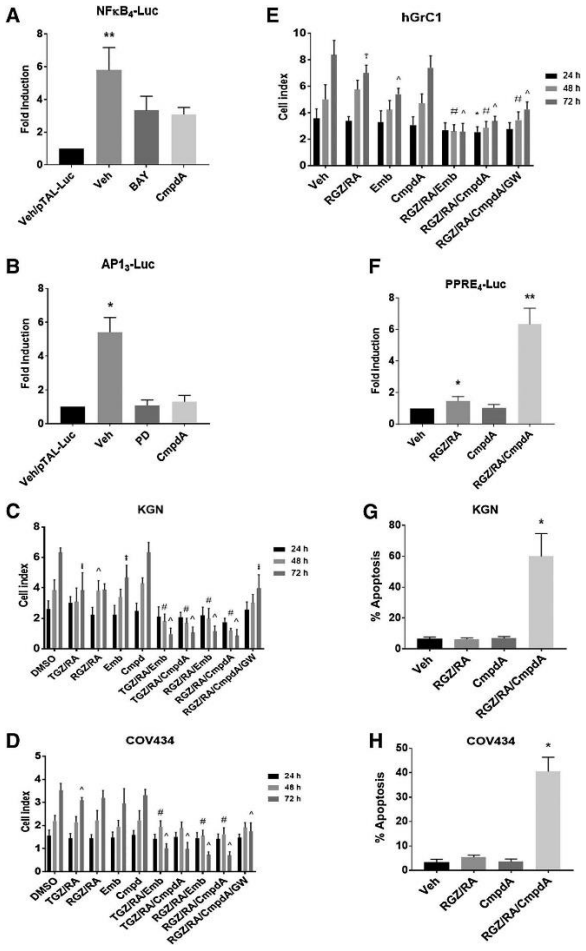

Combined XIAP inhibition and PPARγ activation disrupts KGN 3D spheroid formation

To determine whether the drug combination would be successful in a more physiological setting, we tested combined XIAP inhibition and PPARγ activation in a 3D cell culture model for KGN cells. We observed that the combination treatment (RGZ/RA/CmpdA) at the same concentrations used for the 2D monolayer experiments, caused disruption of spheroid architecture from 24-hour treatment (**Fig. 3A**), with gradual but complete spheroid dissociation occurring over 12-day treatment (**Fig. 3A**). This coincided with a significant decrease in cell viability (**Fig. 3B**) as assessed using the resazurin viability assay.

Combined XIAP inhibition and PPARγ activation disrupts primary patient-derived GCT explants

Combination treatment also disrupted established GCT explants after 7-day treatment, with concomitant loss of cell viability (**Fig. 3C**). We also measured the gene expression levels of stearoyl-CoA desaturase-1 (*SCD*), which encodes the SCD protein that is highly induced after the combination treatment in KGN cells (*Leung DTH et al – concurrent submitted manuscript*). We observed that there was robust induction of *SCD* gene expression after the combination treatment in the explant samples (**Fig. 3D**), indicating that PPARγ is being activated by the combined treatment.

Figure 3

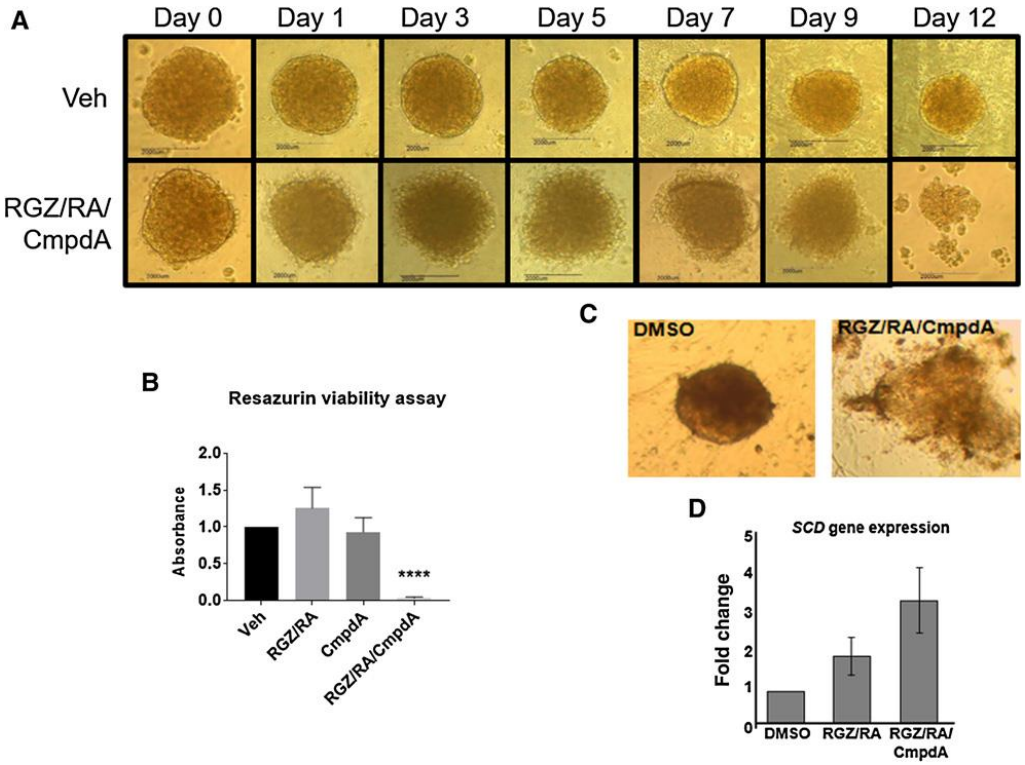

Combined XIAP inhibition and PPARγ activation delayed invasion

To determine whether combined inhibition of XIAP and PPARγ activation can prevent the metastatic process, we used the xCELLigence RTCA system to investigate invasiveness of the KGN cells. We observed that RGZ/RA/CmpdA-treated KGN cells were less invasive than vehicle-treated cells (**Fig. 4A**), with a delayed onset of invasion by 8 hours (**Fig. 4B**).

Combined XIAP inhibition and PPARγ activation decreases mitochondrial respiration and reduces spare respiratory capacity

We next explored the underlying mechanisms of the cytotoxic effect by the combination treatment. Given the pivotal role of mitochondria for energy metabolism in determining cell fate and the association of oxidative stress with the XIAP/Smac signaling pathway, we investigated whether the combined treatment would affect mitochondrial oxygen consumption in the KGN cells. We performed mitochondrial respiratory analysis using Extracellular Flux Analyzer (XFp) to determine whether the oxygen consumption rate (OCR) was altered by the combined treatment. A schematic representation of the design and interpretation of this assay is shown in **Fig. 4C**. OCR was measured every 9 minutes as multiple mitochondrial inhibitors including oligomycin, FCCP, and antimycin A/rotenone were added to the KGN cells in the presence or absence of the treatment. Although RGZ/RA caused a nonsignificant reduction in OCR over the time course of the experiment, the combined XIAP inhibition and PPARγ activation significantly decreased OCR (**Fig. 4D**). By measuring the spare respiratory capacity, which is an estimate of the potential bioenergetic reserve the cell can call upon in times of stress, we observed a significant reduction in the combined treated cells compared with vehicle- or RGZ/RA-treated cells (**Fig. 4E**). This indicates that the combined treatment affected mitochondrial function, inhibiting the ability of the mitochondria to function at their full potential, causing the reserve capacity to be significantly reduced.

TLDA analysis of XIAP inhibition and PPARγ activation in KGN cells

The expression of 93 apoptosis-related genes was analyzed using Taqman Low Density Arrays. Relative gene expression was normalized against the median of geNorm software selected controls. Genes that showed the highest induction after the combined treatment compared to vehicle control were *TNFRSF1B* (TNF Receptor Superfamily Member 1B, 2.3-fold) and *BIRC3* (baculovirus IAP repeat-containing 3 or cIAP2, 139.8-fold).

The induction of these genes, together with TGM2, was validated using qRT-PCR. Cells were treated with DMSO 0.1% (vehicle), PPARγ/RXRα agonists (RGZ/RA 20μM/5μM), Smac-mimetics (Cmpd A and AZD at 500nM) alone and a combination of Smac-mimetics and PPARγ/RXRα agonists. Gene expression is presented as a change in fold induction, relative to *RPLP0* control and normalized to vehicle control. *TNFRSF1B* expression following RGZ/RA treatment alone was not significantly increased. However, *TNFRSF1B* was significantly upregulated following RGZ/RA/CmpdA treatment (**Fig. 4F**). We observed an 8-fold increase of *TGM2* mRNA levels after the combined treatment (**Fig. 4G**). For *BIRC3* mRNA levels, CmpdA and AZD treatments resulted in significantly increased induction when used alone or in combination with RGZ/RA. RGZ/RA treatment did not affect *BIRC3* mRNA levels (**Fig. 4H**).

Figure 4

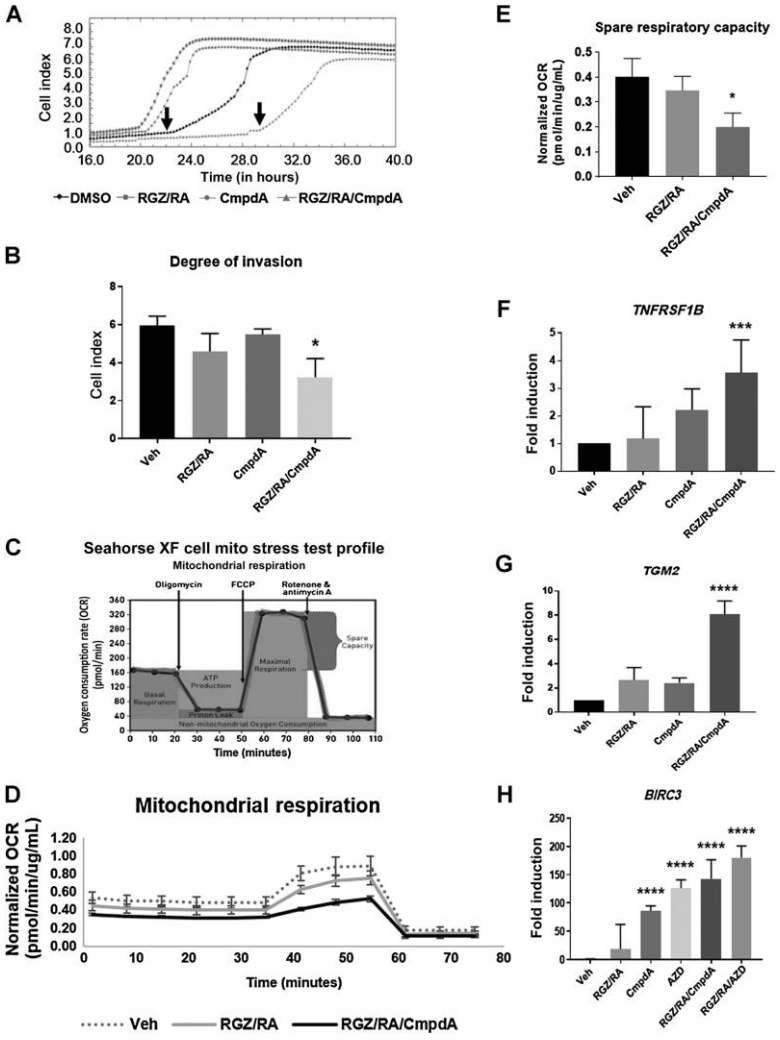

What opportunities for training and professional development has the project provided?

Nothing to report

How were the results disseminated to communities of interest?

We have disseminated findings of our research and publications to:
Granulosa Cell Tumor Research Foundation
Ovarian Cancer Research Foundation
Monash Health Department of Gynaecological Oncology

Newsletters:
https://hudson.org.au/latest-news/one-two-punch-could-knock-out-rare-ovarian-cancer/

What do you plan to do during the next reporting period to accomplish the goals?

We are progressing through Aims 2 and 3 as as described in the Statement of Work.

What was the impact on the development of the principal discipline(s) of the project?

Our findings to show a combination approach using a cancer drug that reduces the granulosa cell tumor's defense mechanisms together with an anti-diabetic drug that attacks the cancer cells. These two drugs are already in clinical or pre-clinical use for other conditions making it likely that we can move quickly from a testing phase into the treatment of this form of ovarian cancer.
The major finding so far is that this combination approach has been effective not only with cell grown in culture flasks, but particularly for cells grown in 3D – which more closely resembles that actual tumor microenvironment. In addition, we have tested the efficacy on surgical tissue samples from GCT patients, that are grown in the dish, and found that the combination approach is just as effective. This has led us to planning in performing these studies in animal models.

What was the impact on other disciplines?

Nothing to Report

What was the impact on technology transfer?

Nothing to Report

What was the impact on society beyond science and technology?

Nothing to Report

5. CHANGES/PROBLEMS:

Nothing to Report

Changes in approach and reasons for change

Actual or anticipated problems or delays and actions or plans to resolve them

<u>Aim 1.1 Developing an in vivo xenograft model</u>

The *in vivo* work outlined in the grant has been delayed due to a number of reasons. The primary delay has been the animal facility located at our Institute has encountered issues centering on construction works of a nearby building that has affected the breeding patterns of animals. The difficulties of performing our work at the Hudson Animal Facility has been a source of frustration, and have caused a delay in my seeking ethics until I have been sure that I can perform the experiments in a suitable facility with minimal likelihood in interruptions to the experiments.

Changes that had a significant impact on expenditures

Nothing to Report

Significant changes in use or care of human subjects, vertebrate animals, biohazards, and/or select agents

Significant changes in use or care of human subjects

Nothing to Report

Significant changes in use or care of vertebrate animals

Nothing to Report

Significant changes in use of biohazards and/or select agents

Nothing to Report

6. PRODUCTS:

- **Publications, conference papers, and presentations**

Journal publications.

Leung DTH, Nguyen T, Oliver EM, Matti J, Alexiadis M, Silke J, Jobling TW, Fuller PJ, Chu S. Combined PPARγ Activation and XIAP Inhibition as a Potential Therapeutic Strategy for Ovarian Granulosa Cell Tumors. Mol Cancer Ther. 2019 18(2):364-375. doi: 10.1158/1535-7163.MCT-18-0078. PMID: 30530769.
acknowledgement of federal support: Yes

Leung DTH, Rainczuk A, Nguyen T, Stephens A, Silke J, Fuller PJ, Chu S. Targeting XIAP and PPARγ in Granulosa Cell Tumors Alters Metabolic Signaling. J Proteome Res. 2019 5;18(4):1691-1702. doi: 10.1021/acs.jproteome.8b00917. PMID: 30706710.
acknowledgement of federal support: Yes

Books or other non-periodical, one-time publications.

Leung DTH, Chu S. Measurement of Oxidative Stress: Mitochondrial Function Using the Seahorse System. Methods Mol Biol. 2018;1710:285-293. doi: 10.1007/978-1-4939-7498-6_22. PMID: 29197011.
acknowledgement of federal support: No

Other publications, conference papers, and presentations

European Society of Gynaecological Oncology State of the Art Conference "New Insights in Rare Gynaecological Malignancies", Lyon, France October 4-6 2018
Abstract 3983: PPARgamma Activation and XIAP Inhibition Mutually Augment their respective Anticancer Effects in Granulosa Cell Tumors of the Ovary. Simon Chu, Dilys Leung, Trang Nguyen, Maria Alexiadis, Peter Fuller

Abstract 3987: Mutational Landscape of Adult Granulosa Cell Tumors of the Ovary from Whole Exome Sequencing. Simon Chu, Maria Alexiadis, Dilys Leung, Simone Rowley, Ian Campbell, Peter Fuller

- **Website(s) or other Internet site(s)**

https://hudson.org.au/latest-news/one-two-punch-could-knock-out-rare-ovarian-cancer/

- **Technologies or techniques**

Nothing to Report

- **Inventions, patent applications, and/or licenses**

Nothing to Report

- **Other Products**

Nothing to Report

7. PARTICIPANTS & OTHER COLLABORATING ORGANIZATIONS

What individuals have worked on the project?

Name:	Trang Nguyen
Project Role:	Research Assistant
Months worked:	27 months
Contribution to Project:	Ms Nguyen performed RNA-Seq, ChIP, and XIAP knockout experiments, performs all Tissue Culture experiments. She will be involved in the in vivo experiments beginning 2021.
Name:	Maria Alexiadis
Project Role:	Senior Research Assistant (0.5 FTE)
Months worked:	12 months
Contribution to Project:	Ms Alexiadis is performing Bioinformatic analysis for our RNA-Seq data, proteomic analysis of SILAC experiments, and will be analyzing the ChIP-Seq data once performed in conjunction with Professor George Muscat.

Has there been a change in the active other support of the PD/PI(s) or senior/key personnel since the last reporting period?

Nothing to Report

What other organizations were involved as partners?

Nothing to Report

8. SPECIAL REPORTING REQUIREMENTS

COLLABORATIVE AWARDS:

QUAD CHARTS:

9. APPENDICES:

Attached are 2 original publications

Leung DTH, Nguyen T, Oliver EM, Matti J, Alexiadis M, Silke J, Jobling TW, Fuller PJ, Chu S. Combined PPARγ Activation and XIAP Inhibition as a Potential Therapeutic Strategy for Ovarian Granulosa Cell Tumors. Mol Cancer Ther. 2019 18(2):364-375. doi: 10.1158/1535-7163.MCT-18-0078. PMID: 30530769.
Acknowledgement of federal support: Yes

Leung DTH, Rainczuk A, Nguyen T, Stephens A, Silke J, Fuller PJ, Chu S. Targeting XIAP and PPARγ in Granulosa Cell Tumors Alters Metabolic Signaling. J Proteome Res. 2019 5;18(4):1691-1702. doi: 10.1021/acs.jproteome.8b00917. PMID: 30706710.
Acknowledgement of federal support: Yes

Published OnlineFirst December 7, 2018; DOI: 10.1158/1535-7163.MCT-18-0078

Cancer Biology and Translational Studies

Molecular Cancer Therapeutics

Combined PPARγ Activation and XIAP Inhibition as a Potential Therapeutic Strategy for Ovarian Granulosa Cell Tumors

Dilys T.H. Leung[1], Trang Nguyen[1], Edwina May Oliver[1], Juliana Matti[1], Maria Alexiadis[1], John Silke[2], Thomas W. Jobling[3], Peter J. Fuller[1], and Simon Chu[1]

Abstract

Ovarian granulosa cell tumors (GCT) are characterized by indolent growth and late relapse. No therapeutic modalities aside from surgery have proven effective. We previously reported overexpression of the nuclear receptor, peroxisome proliferator-activated receptor-gamma (PPARγ), and constitutive activity of the NFκB and AP1 signaling pathways in GCT. PPARγ presents as a potential therapeutic target as it impedes proliferation and promotes terminal differentiation of granulosa cells. However, resistance to the actions of PPARγ is caused by NFκB transrepression in GCT-derived cell lines, KGN and COV434. We showed that abrogation of NFκB signaling in GCT cells enables PPARγ agonists to initiate apoptosis. In addition, we observed overexpression of an NFκB–induced gene, X-linked inhibitor of apoptosis protein (XIAP), in GCT and GCT-derived cells. XIAP is an attractive therapeutic target due to its role in inhibiting the apoptotic pathway. We investigated the antitumor effects of combined XIAP inhibition using Smac-mimetics and PPARγ activation using thiazolidinediones (TZD) in the GCT-derived cells. Transactivation assays revealed that NFκB transrepression of PPARγ can be relieved by NFκB or XIAP inhibition. Combined Smac-mimetic and TZD significantly induced apoptosis, reduced cell viability and proliferation in KGN cells in monolayer and 3D spheroid culture, and in GCT explant models. The Smac-mimetic and TZD cotreatment also delayed cell invasion, upregulated proapoptotic genes, and compromised cell metabolism in KGN cells. This study provides evidence that PPARγ and XIAP cotreatment has antineoplastic effects in GCT. As therapeutics that target these proteins are already in clinical or preclinical use, expedient translation to the clinic is possible.

Introduction

Granulosa cell tumors (GCT), which comprise the majority of ovarian stromal tumors, arise from proliferating granulosa cells (GC) of the ovarian follicle, and represent a specific subset of malignant ovarian tumors (1). They frequently present with endocrine manifestations such as estrogenization in prepubertal girls and postmenopausal women. GCTs exhibit many features of normal ovarian GCs (1), including expression of the follicle stimulating hormone (FSH) receptor gene, estrogen synthesis, estrogen receptor (ER) β expression, inhibin subunit expression with synthesis of biologically active inhibin, and anti-Müllerian hormone (AMH) expression. The adult form of GCT (95%) are defined by the presence of the *FOXL2* C134W mutation, which is absent in the juvenile subtype (5%). GCTs exhibit an indolent course and have an unexplained propensity for late recurrence; approximately 80% of patients with aggressive or recurrent tumors die from their disease (1). Currently, there are no reliable methods for predicting relapse and, aside from surgery, therapeutic modalities are limited (1).

Nuclear receptors (NR) play a central pathogenic role in several endocrine malignancies and as such represent established therapeutic targets. We have previously shown that peroxisome proliferator-activated receptor-gamma (PPARγ) is highly expressed in GCT (2). PPARγ is implicated in the pathology of numerous diseases including obesity and diabetes. PPARγ binds to DNA at specific sites as an obligate functional heterodimer with retinoid X receptor-alpha (RXRα), which is also expressed in GCT and in two GCT-derived cell lines (2). The potential of PPARγ agonists as anticancer agents has attracted considerable interest, including the treatment of endocrine malignancies such as thyroid, prostate, and pancreatic cancer (NCT00098852; NCT00182052; NCT02475499; https://clinicaltrials.gov/).

The role of the NFκB family of proteins in immune, inflammatory, and antiapoptotic responses is well documented (3, 4). NFκB and the signaling pathways that are involved in its activation are also important for tumor development; activated NFκB increases the expression of genes involved in cell proliferation, metastasis, and antiapoptosis (5). In GCT, we have previously demonstrated that constitutive NFκB signaling transrepresses several NR (6). Reciprocal transrepression of NFκB and NR is well described (7), usually as a consequence of protein–protein interaction without direct binding to DNA. The best characterized

[1]Hudson Institute of Medical Research and the Monash University Department of Molecular and Translational Science, Clayton, Victoria, Australia. [2]Walter and Eliza Hall Institute of Medical Research, Parkville, Victoria, Australia. [3]Department of Gynecology Oncology, Monash Health, Clayton, Victoria, Australia.

Note: Supplementary data for this article are available at Molecular Cancer Therapeutics Online (http://mct.aacrjournals.org/).

Corresponding Author: Simon Chu, Hudson Institute of Medical Research, 27-31 Wright Street, Clayton, Victoria 3168, Australia. Phone: 61-3-8572-2545; Fax: 61-3-9594-6125; E-mail: simon.chu@hudson.org.au

doi: 10.1158/1535-7163.MCT-18-0078

Published OnlineFirst December 7, 2018; DOI: 10.1158/1535-7163.MCT-18-0078

interactions are those of NFκB and the glucocorticoid receptor (GR), while the androgen and progesterone receptors also physically interact with NFκB (7).

Apoptosis is induced by activated caspases. The inhibitors of apoptosis proteins (IAP) family are antiapoptotic regulators, several of which have been shown to be upregulated in various cancers. These proteins are characterized by the presence of baculovirus IAP repeat (BIR) domains, which are responsible for inhibiting caspases. The best characterized IAP is the X-linked inhibitor of apoptosis protein (XIAP) and is the most potent caspase inhibitor (8). XIAP has three BIR domains, and a RING finger domain conferring E3-ubiquitin ligase activity (8). XIAP is predominantly regulated by the mitochondrial protein, Second mitochondria-derived activator of caspases/direct IAP-binding protein with low pI (Smac/DIABLO; refs. 9, 10). When mitochondria become compromised and apoptosis is triggered, Smac is released into the cytoplasm where it binds to the caspase-binding domains of XIAP. This subsequently displaces activated caspases to promote apoptosis (8). Thus, XIAP is an attractive therapeutic target for novel anticancer treatment (11, 12). Clinical trials for small-molecule inhibitors of XIAP tested alone or in combination with other chemotherapy have been outlined in Fulda (2015) (12). This includes trials in solid tumors including head and neck carcinomas, breast and ovarian cancers, as well as hematologic malignancies such as lymphoma and leukemia. In this study, we investigated the effects of PPARγ agonists on GCT-derived cells *in vitro*, and showed that when combined with Smac-mimetics, they release transrepression of PPARγ by NFκB, resulting in an induction of apoptosis.

Materials and Methods

Patients, tissue acquisition, and tissue microarray

We used previously characterized ovarian adult GCT samples (all *FOXL2* mutation positive; $n = 14$) collected sequentially at our institution (2, 13–15). Normal ovarian tissue was obtained from 8 premenopausal women who had undergone elective hysterectomy with oophorectomy for conditions not associated with ovarian malignancy. Tissue microarrays (TMA) were provided by Professor Colin Stewart (University of Western Australia, Perth, Australia). The study protocol was approved by the Research and Ethics Committee of Monash Medical Centre (Clayton, Australia) and all women gave written informed consent for the studies.

Cell lines

Cell lines used in these studies are the human GCT-derived cells, COV434 and KGN (16, 17), and the human nonluteinized granulosa cell line, hGrC1 (18). The KGN cells are heterozygous for the FOXL2 mutation and hence derived from an adult GCT. The COV434 cells are wild type for FOXL2, representing a juvenile GCT model (1). The KGN and COV434 cell lines were purchased from and authenticated by ATCC (www.atcc.org). These cell lines have been authenticated by molecular profiling of the short tandem repeats using the PowerPlex 16 HS System PCR Amplification Kit, and data matched through searching cell line data extracted from both ATCC and HyperCLDB. The hGrC1 cells were obtained in 2014 from Bayasula (2012; ref. 18) who established this cell line. Cells were maintained in DMEM/F12 (KGN) or DMEM (COV434 and hGrC1) supplemented with 10% FCS at 37°C in a 95% air/5% CO_2 humidified incubator. All cell lines were tested negative for *Mycoplasma* (MycoAlert PLUS Mycoplasma Detection Kit, Lonza) in October 2015 prior to the experiments. *In vitro* experiments were typically completed within 5 passages.

Chemicals and antibodies

PPARγ agonists and antagonist used were troglitazone (TGZ), rosiglitazone (RGZ), and GW9662 (Sigma-Aldrich; ref. 19). Chemical inhibitors used were BAY11-7082 (20) and PD-98059 (Sigma-Aldrich; ref. 21); XIAP inhibitors: Compound A (a bivalent Smac-mimetic; CmpdA; ref. 22); AZD5582 (monovalent Smac-mimetic; AZD; Tocris Bioscience; ref. 23); embelin (2,5-dihydroxy-3-undecyl-1,4-benzoquinone; Sigma-Aldrich; ref. 24). High Content Screening dyes were Hoechst 33342, YoPro-1, and ToPro-3 (Life Technologies).

Antibodies used were as follows: PPARγ (ab27649), cIAP1 (ab2399; Abcam), XIAP (PRS3331; Sigma-Aldrich), and cIAP2 (sc-7944; Santa-Cruz Biotechnology).

xCELLigence proliferation assay

Cell proliferation was assessed in a real-time, noninvasive, and label-free manner using the xCELLigence Real-Time Cell Analyzer (RTCA) DP apparatus (Acea Biosciences). Proliferation was assessed as per the manufacturer's instructions. Briefly, 1×10^4 KGN cells were seeded in each well of an E-plate 96 in a total volume of 100 μL of 2% charcoal-stripped serum media. Cell index as a measure of proliferation was assessed every 2 to 15 minutes for 120 hours. Each condition was performed in triplicate. Drugs were not replenished over the course of experiment; the experiment was terminated at approximately 120 hours, and data were collected for analysis. Relative cell proliferation is presented by the final cell index, which is calculated by the difference between the resistance generated by the cells in each time point and the resistance of the medium without cells.

The xCELLigence RTCA system was also utilized to assess invasion of the KGN cells. Electrical current passes through the electrodes on the bottom of the upper chamber of the cell culture plate (CEM-16). As cells seeded in the upper chamber invaded across a layer of Matrigel into the lower chamber, which contains 10% FCS as chemoattractant, they attach onto the electrodes and electrode resistances increase. The electrode resistance is indicative of cell invasion and is represented by cell index. The maximum cell indices across a 72-hour period, which is indicative of number of cells invaded, were compared between the control and treatment groups.

High content screening apoptosis assays

Cells were grown in 24-well plates and treated for 24 hours. Media containing Hoechst 33342 dye, YoPro-1 dye (to detect early apoptosis), and ToPro-3 dye (to detect late apoptosis or necrosis) were added to the cells before imaging and analyzed on a Cellomics ArrayScan VTI High Content Screening Reader (Thermo Fisher Scientific).

Reverse transcription and real time RT-PCR

The comparative C_t ($\Delta\Delta C_t$) method was used to validate XIAP expression. Fluorescein amidite (FAM) labeled TaqMan Gene Expression assays for X-linked inhibitor of apoptosis protein (*XIAP*), TNFR superfamily 1B (*TNFRSF1B*), baculovirus IAP

Published OnlineFirst December 7, 2018; DOI: 10.1158/1535-7163.MCT-18-0078

repeat-containing protein 3 (*BIRC3*), and transglutaminase 2 (*TGM2*) were purchased along with an endogenous control probe, FAM labeled 60S acidic ribosomal protein P0 (*RPLP0*) probe. A 10 μL reaction was prepared with 1× TaqMan universal PCR Master Mix (Applied Biosystems) and diluted cDNA. All PCR reactions were carried out in triplicate in MicroAmp optical 384-well reaction plates (Applied Biosystems). The cycling parameters were initiated by 2 minutes at 50°C and 10 minutes at 95°C, followed by 40 cycles of 15 seconds at 95°C and 60°C for 1 minute using the 7900HT fast real-time PCR system (Applied Biosystems).

TaqMan low-density array

A TaqMan low-density array (Applied Biosystems #4378701) containing gene expression assays for 93 apoptosis genes and 3 internal controls [eukaryotic 18S rRNA (*18S*), *GAPDH* and β-actin (*ACTB*)] was used to profile gene expression. Total RNA (1.5 μg) was reverse-transcribed using random hexamers with SuperScript III reverse transcriptase (Invitrogen, Thermo Fisher Scientific). The arrays were processed and analyzed in accordance with the manufacturer's protocols as described previously (2). Each GCT sample was run once while the cell lines were run as three biological replicates.

IHC

Four-micron sections of OCT (optimal cutting temperature)-embedded frozen GCT were prepared. All incubation and washes were performed at room temperature unless stated otherwise. The frozen GCT sections were fixed in 4% paraformaldehyde and endogenous peroxidase quenched using 0.3% hydrogen peroxide/PBS. Triton X-100/PBS (0.1%) was used for membrane permeation. Nonspecific binding was blocked by 10% goat serum in 3% BSA for 1 hour. Incubation with primary antibody, rabbit polyclonal PPARγ (Abcam ab27649; 1:350), XIAP (Sigma-Aldrich PRS3331; 1:200), or goat serum (negative control) was performed at 4°C overnight. After PBS washes, slides were incubated with biotinylated goat anti-rabbit secondary antibody (Dako, Agilent Technologies; 1:200) for an hour. Avidin/biotinylated enzyme complex (Vector Laboratories) was added to sections and incubated for an hour. Staining was visualized by incubation of DAB solution (Dako) for 3 minutes. Sections were counterstained with hematoxylin and dehydrated (70% and 100% ethanol). Staining was analyzed using "positive pixel count v9" algorithm in the Aperio ImageScope version 12.3.0.5056 (Leica Biosystems). Percentage of positive (brown) staining indicating protein levels was determined as low (0%–30%), medium (31%–79%), or high (>80%).

Transactivation assays

The KGN cells were transfected using SuperFect reagent (Qiagen) as described previously (6). The reporter constructs, $NF\kappa B_4$-luc or $AP1_3$-luc, were transfected in the KGN cells and then treated for 24 hours with DMSO (0.1%) as vehicle control, CmpdA (500 nmol/L), BAY11-7082 (5 μmol/L), or PD98059 (20 μmol/L) to inhibit either NFκB or AP1.

Extracellular flux assay

Cellular bioenergetic profiling of the KGN cells was assessed using the Seahorse XF Cell Mito Stress Test Kit. Briefly, the sensor cartridge was hydrated with calibrant overnight prior to cell seeding. KGN cells (1×10^4) were plated in 6 wells, with 2 further wells containing media only for background correction. Following 24-hour treatments, cells were washed twice with the XFp base medium (supplemented with 1 mmol/L pyruvate, 2 mmol/L glutamine, and 10 mmol/L glucose). Stressors were prepared in XFp base medium with oligomycin (1 μmol/L), FCCP (2 μmol/L), or antimycin A/rotenone (0.5 μmol/L). Cellular bioenergetics was measured on a Seahorse Extracellular Flux XFp Analyzer according to the manufacturer's protocol. Pierce BCA protein assay (Thermo Fisher Scientific) was performed for normalization. Data analysis was performed with the analyzer's Wave software version 2.3.0.20.

Spheroid formation assay

To generate spheroids, 3,000 KGN cells were seeded in DMEM/F12 with 20% methylcellulose and without additives or serum. Spheroids formed within 24 to 72 hours postseeding. Spheroids were treated in quadruplicate in 2% charcoal-stripped serum-containing DMEM/F12, and replenished every 3 days. Cell viability was assessed using 0.005% resazurin (Sigma-Aldrich) in 2% charcoal-stripped FCS-containing DMEM/F12. Fluorescence signal was measured using excitation at 560 nm and emission at 595 nm (25).

Primary GCT culture

Primary GCTs collected from oophorectomy of two women were each dissected into three 1-mm^3 pieces, plated in a 6-well plate, and treated in 10% serum-containing DMEM/F12 for 24 hours. Following treatment, the explant culture was pooled to extract RNA for further analysis.

Statistical analysis

Drug treatments for all experiments were performed in duplicates and repeated at least three times. Data are presented as mean ± SD. Student's *t* test, one-way ANOVA, or the nonparametric equivalent, Kruskal–Wallis test was used for statistical analyses where $P < 0.05$ is considered statistically significant.

Results

Expression of XIAP and PPARγ in GCT and GCT-derived cell lines

We have previously described *PPARγ* mRNA overexpression in GCT ($n = 12$) and the GCT-derived cell lines, KGN and COV434 (2). We performed expression profiles for 12 tumors, and also for the KGN and COV434 cell lines. The GCT samples for RT-PCR analysis have been described previously (2, 13–15).

Using quantitative RT-PCR, we observed that *XIAP* was abundantly expressed in the cell lines and was significantly upregulated in GCT compared with whole normal ovary samples (Fig. 1A). *XIAP* mRNA expression did not differ between stage I and advanced stage GCT (Supplementary Fig. S1). The expression of XIAP and PPARγ was also examined at the protein level using IHC, which demonstrated strong staining for both proteins (Fig. 1B). TMA analysis revealed that XIAP expression was high in 52 of 76 (68%) of the primary tumor samples (Fig. 1C; Table 1). For those tumor samples with both primary and recurrent cores, we observed that XIAP expression did not differ between tumor samples (Table 1). The TMA included a normal preovulatory ovarian sample with moderate level of XIAP expression, where

Published OnlineFirst December 7, 2018; DOI: 10.1158/1535-7163.MCT-18-0078

staining was observed in the granulosa cells of both small follicles and a preovulatory follicle, as well as in the surrounding theca (Fig. 1C).

We observed very low expression of cIAP1 in all tissues examined, whereas no expression of cIAP2 was observed (Fig. 1C).

Consistent with our previous observation of high *PPARγ* mRNA levels (2), we observed high levels with IHC for PPARγ in the majority of the GCT cores in the TMA. Moderate to high expression of PPARγ was observed for 49 of 76 (64%) of primary GCTs (Fig. 1C; Table 1). Normal preovulatory ovarian samples showed moderate expression of PPARγ; nuclear staining was observed in the granulosa cells of the small and preovulatory follicle, whereas both nuclear and cytoplasmic staining were observed in the cells of the surrounding stroma (Fig. 1C).

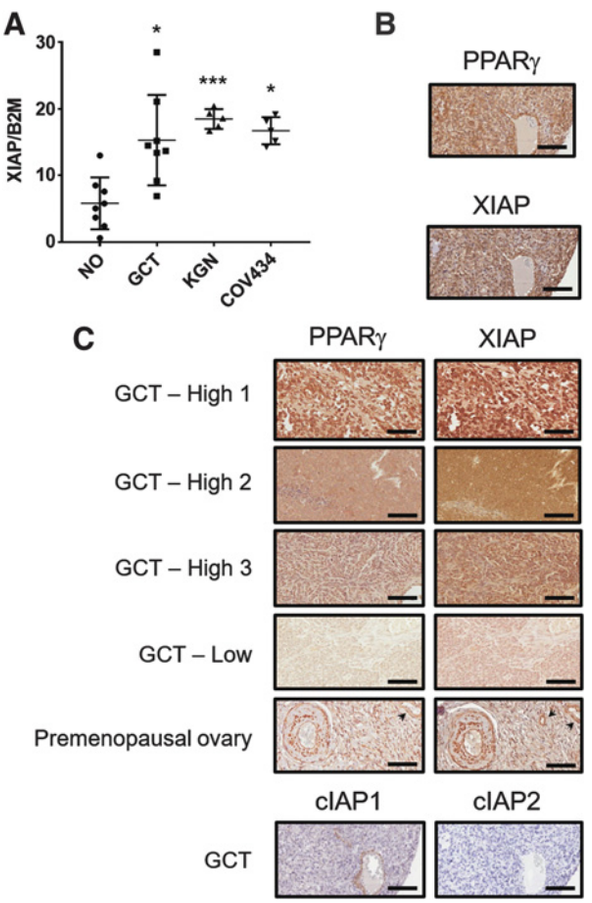

Figure 1.

mRNA and protein expression in GCT, GCT-derived cell lines, and premenopausal ovaries. **A,** *XIAP* mRNA level was assessed using RT-PCR. The panel includes 8 premenopausal ovary (NO), 8 GCT, and the two human GCT-derived cell lines, KGN and COV434. Mean ± SD. Kruskal–Wallis; Dunn's *post hoc* analysis; *, $P < 0.05$; ***, $P < 0.001$ when compared with NO. **B,** PPARγ and XIAP protein expression in GCT was determined using IHC. **C,** High to low expression of XIAP and PPARγ was observed in the GCT cores in the TMA. XIAP and PPARγ was also detected in the granulosa cells and theca cells in a normal premenopausal ovarian sample. Very low levels of cIAP1 and no expression of cIAP2 was observed in GCT samples.

NFκB causes transrepression of PPARγ in GC- and GCT-derived cell lines

In KGN cells, activation of PPARγ and RXRα using the PPARγ agonist, RGZ (20 μmol/L), and the RXRα agonist, 9-*cis*-retinoic acid (RA; 5μmol/L), resulted in a nonsignificant 30% reduction in cell proliferation compared with vehicle (Fig. 2A). When cells were transfected with a PPARγ reporter construct ($PPRE_4$-luciferase) and treated with RGZ/RA, there was a small activation of the reporter compared with vehicle (Fig. 2B). However, after 24 hours of RGZ/RA treatment, no significant increase in apoptosis was observed for either KGN or COV434 cells (Fig. 2C and D). A sublethal dose of the NFκB inhibitor, BAY11-7082 (BAY; 2 μmol/L) alone, did not affect cell proliferation (Fig. 2A) or activate the PPARγ reporter (Fig. 2B). When RGZ/RA was combined with BAY, proliferation was blocked (Fig. 2A) with a significant increase in apoptosis (Fig. 2C and D). This response was likely mediated by PPARγ as the effect was reversed by the PPARγ antagonist, GW9662 (GW; 20 μmol/L; Fig. 2A). The robust activation of the reporter by RGZ/RA in combination with BAY (Fig. 2B) indicated that NFκB transrepressed PPARγ signaling. Similar results were observed when another PPARγ agonist, TGZ, was used in these assays (Supplementary Fig. S2A–S2D).

Inhibiting XIAP decreases NFκB and AP1 transactivation

We previously reported that the NFκB and AP1 signaling pathways are constitutively activated in KGN and COV434 cells (6). NFκB transcriptionally activates XIAP expression, while XIAP modulates NFκB activation as a consequence of a positive feed-forward loop. XIAP has been reported to regulate NFκB through the ubiquitin ligase activity of its RING domain (26). XIAP also activates NFκB and AP1 signaling pathways via the activation of TGFβ-activated kinase 1 (TAK1; ref. 27). In addition to the removal of PPARγ transrepression, we thus sought to determine if inhibiting XIAP could also decrease the constitutive activity of NFκB and AP1 in the GCT-derived cell lines. When cells were transfected with either a NFκB or AP1 reporter, there was an approximate 6-fold induction of luciferase activity under basal conditions compared with cells transfected with an enhancer-less reporter (pTAL-Luc; Fig. 3A and B). Treating KGN cells with 5 μmol/L BAY11-7082 or 20 μmol/L PD-98059 (PD; ERK/AP1 inhibitor) suppressed the respective constitutive activity as reported previously (6). When we treated KGN cells with a Smac-mimetic, CmpdA (500 nmol/L), the constitutive

Table 1. XIAP and PPARγ protein expression on GCT tissue microarray[a]

	GCT tissue microarray ($n = 76$: 52 primary tumors only; 4 recurrent tumors only)[b]	
	Low	Medium/high
Marker	***n* (%)**	***n* (%)**
XIAP	24 (32)	52 (68)
PPARγ	27 (36)	49 (64)

[a]Staining was analyzed using "positive pixel count v9" algorithm in the Aperio ImageScope version 12.3.0.5056 (Leica Biosystems). Percentage of positive (brown) staining indicating protein levels was determined as low (0%–30%), medium (31%–79%), or high (>80%).

[b]Each sample represents a GCT collected from an individual patient. Of the 52 primary tumors, 20 have multiple samples and 4 patients have developed recurrent diseases, which were included in the cohort. The tumor samples with both primary and recurrent cores were scored medium/high for XIAP and PPARγ expression.

Published OnlineFirst December 7, 2018; DOI: 10.1158/1535-7163.MCT-18-0078

activity was abrogated for both pathways, indicating that XIAP is regulating both pathways, potentially through the TAK1–TAB1/2/3 complex (Fig. 3A and B). A similar result was observed for the COV434 cell line (Supplementary Fig. S3A and S3B).

XIAP inhibition prevents NFκB transrepression and potently sensitizes KGN and COV434 cells to PPARγ-mediated apoptosis

As inhibition of XIAP abrogates the constitutive activity of both the NFκB and AP1 signaling pathways, we hypothesized that inhibition of XIAP would remove NFκB-mediated transrepression of PPARγ. Using the xCELLigence RTCA system to assess cell proliferation in real time, we assessed the effect of CmpdA (500 nmol/L) either as a single treatment, or in combination with the PPARγ agonists KGN and COV434 cells, and in a nonluteinized granulosa cell line, hGrC1. When cells were treated with CmpdA alone, there was no effect on cell proliferation for either the GCT-derived cell lines (Fig. 3C and D) or the hGrC1 cells (Fig. 3E) over 72 hours. In addition, CmpdA alone also had no effect on PPARγ transactivation (Fig. 3F) or apoptosis (Fig. 3G and H). PPARγ activation alone with RGZ/RA or TGZ/RA caused a small decrease in proliferation (Fig. 3C–E) with no effect on apoptosis (Fig. 3G and H). Combining CmpdA and with RGZ/RA (20 μmol/L/5 μmol/L) resulted in cessation of cell proliferation in both KGN (Fig. 3C) and COV434 (Fig. 3D) cells over 72 hours. This was accompanied by robust PPARγ-mediated transactivation of the reporter construct (Fig. 3F) and significant increase in apoptosis (Fig. 3G and H), similar to that seen with combined NFκB inhibition and PPARγ activation (Fig. 2B–D). Consistent results were observed when a monomeric Smac-mimetic AZD5582 was used in combination with RGZ/RA or with another PPARγ agonist, TGZ (Supplementary Fig. S3C–S3F).

Combined XIAP inhibition and PPARγ activation disrupts KGN 3D spheroid formation

To determine whether the drug combination would be successful in a more physiologic setting, we tested combined XIAP inhibition and PPARγ activation in a 3D cell culture model (25)

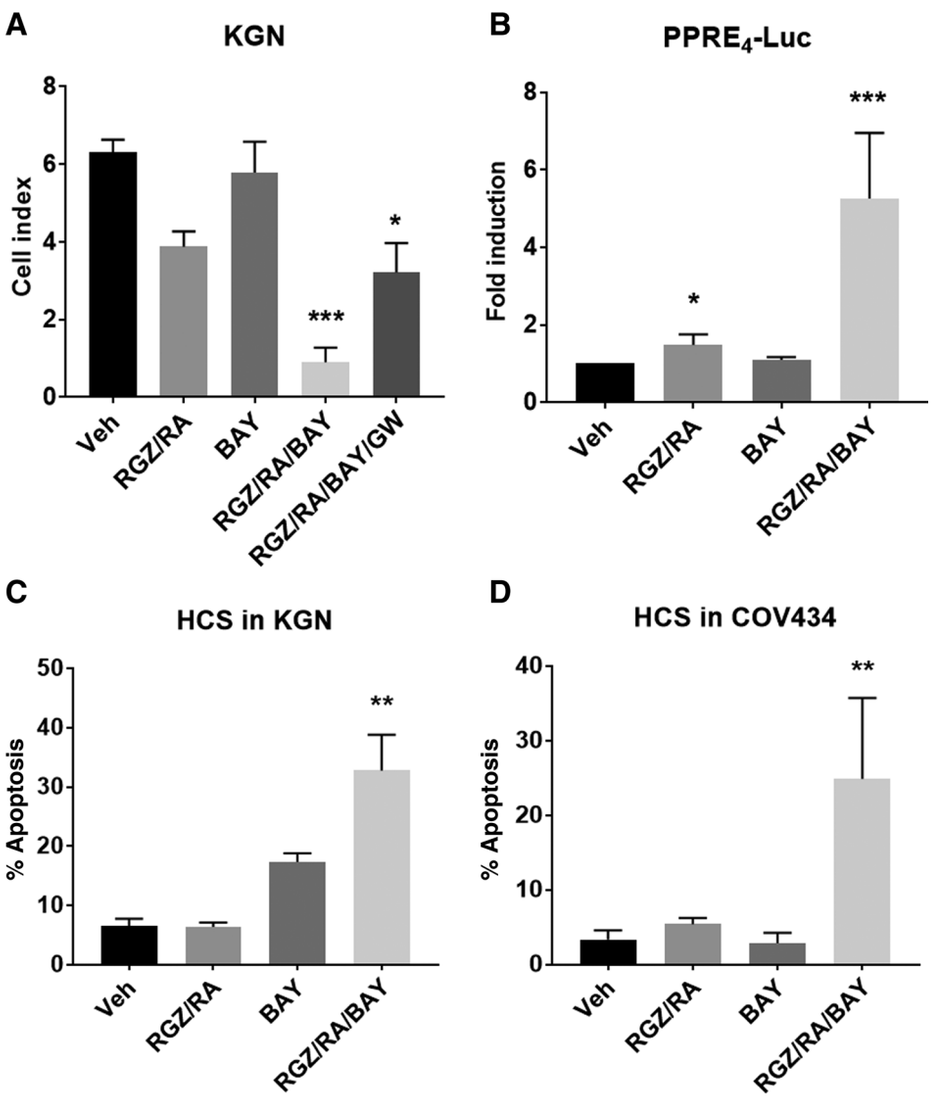

Figure 2.
Effects of PPARγ activation. RGZ (20 μmol/L) and RA (5 μmol/L) were used to activate PPARγ in the KGN and COV434 cells. GW9662 (GW; 20 μmol/L) is a PPARγ antagonist used to reverse the effects of PPARγ activation. The effect of PPARγ activation on proliferation (**A**), PPARγ-mediated transactivation (**B**), and apoptosis (**C** and **D**) was investigated. One-way ANOVA; Tukey *post hoc* analysis; *, $P < 0.05$; **, $P < 0.01$; ***, $P < 0.001$ compared with vehicle (Veh; 0.1% DMSO) at 24 hours. $n = 3$ in duplicate wells.

Published OnlineFirst December 7, 2018; DOI: 10.1158/1535-7163.MCT-18-0078

for KGN cells. We observed that the combination treatment (RGZ/RA/CmpdA) at the same concentrations used for the 2D monolayer experiments, caused disruption of spheroid architecture from 24-hour treatment, with gradual but complete spheroid dissociation occurring over 12-day treatment (Fig. 4A). Singular treatments, RGZ/RA and CmpdA, have no effects on the spheroids (Supplementary Fig. S4). This coincided with a significant decrease in cell viability (Fig. 4B) as assessed using the resazurin viability assay.

Combined XIAP inhibition and PPARγ activation disrupts primary patient-derived GCT explants

Combination treatment also disrupted established GCT explants after 7-day treatment, with concomitant loss of cell

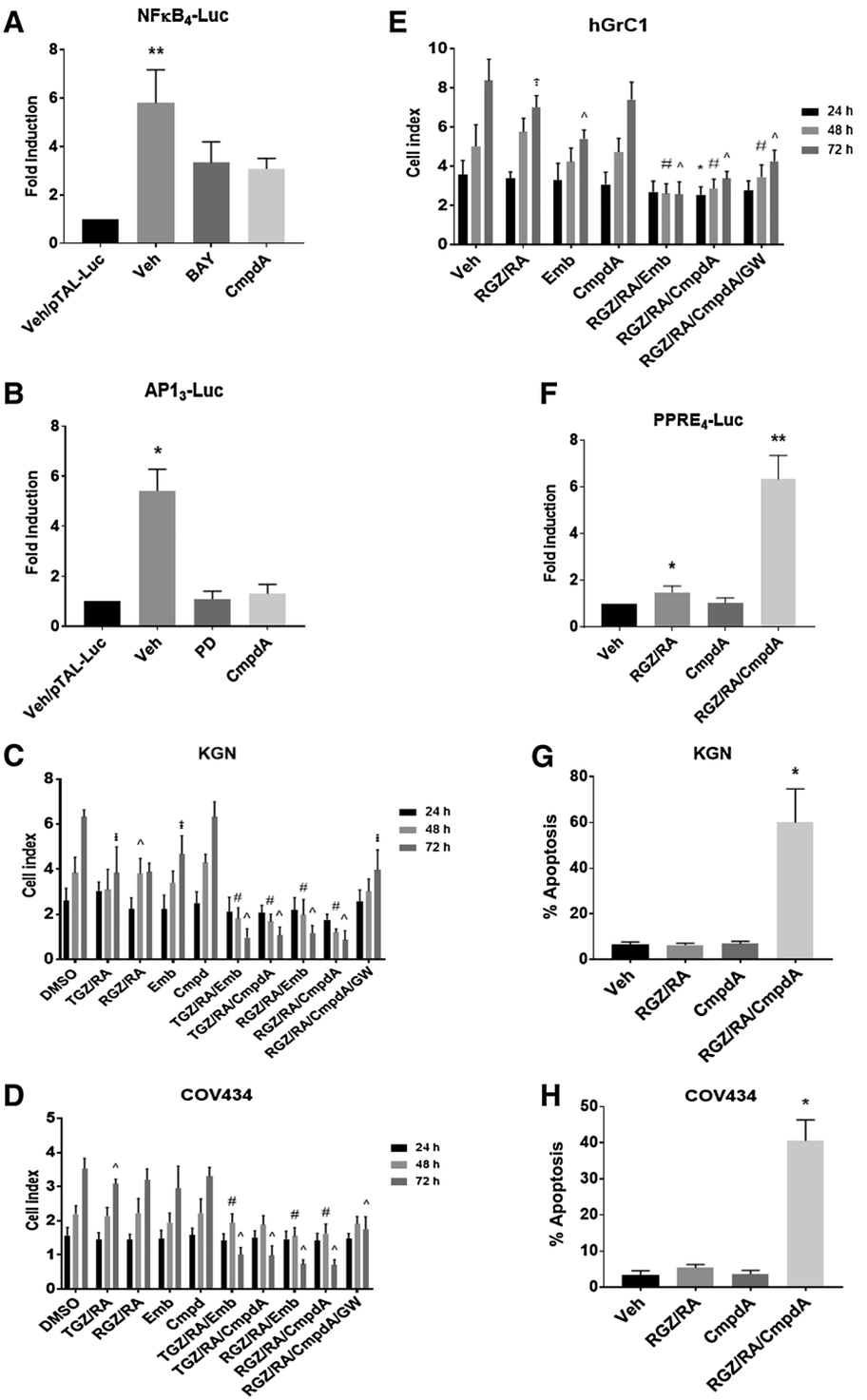

Figure 3.

Effects of PAPRγ activation and XIAP inhibition. **A** and **B,** XIAP inhibition with CmpdA in transactivation assays. The KGN cells were transfected with an NFκB (**A**) or AP1 (**B**) reporter, or an enhancer-less reporter, pTAL-Luc (pTAL). The cells were treated with the NFκB inhibitor (**A**), BAY11-7082 (BAY), or ERK/AP1 inhibitor (**B**), PD-98095 (PD), to suppress the respective constitutive activity. $n = 4$ in duplicate wells. **C–E,** Proliferation assay. TGZ or RGZ (20 μmol/L) and RA (5 μmol/L) were used to activate PPARγ alone or in combination with 10 μmol/L Emb or 500 nmol/L CmpdA to inhibit XIAP in the KGN (**C**), COV434 (**D**), and hGrC1 (**E**) cells for 24 to 72 hours. GW9662 (GW; 20 μmol/L) is a PPARγ antagonist used to reverse the effects of PPARγ activation. *, $P < 0.05$ compared with vehicle (Veh; 0.1% DMSO) at 24 hours; #, $P < 0.01$ compared with Veh at 48 hours; †, $P < 0.05$ compared with Veh at 72 hours; ^, $P < 0.01$ compared with Veh at 72 hours. $n = 3$ in duplicate wells. **F,** PPARγ-mediated transactivation in KGN. Cells were treated with RGZ/RA in combination with CmpdA. $n = 5$ in duplicate wells. **G** and **H,** High content screening. Apoptosis was assessed after 24-hour of RGZ/RA and CmpdA in single or combined treatment in the KGN (**G**) and COV434 (**H**) cells. $n = 5$ in triplicate wells. *, $P < 0.05$; **, $P < 0.01$ when compared with vehicle. Mean ± SD. All statistical analyses were performed using Kruskal–Wallis test and Dunn *post hoc* analysis.

Published OnlineFirst December 7, 2018; DOI: 10.1158/1535-7163.MCT-18-0078

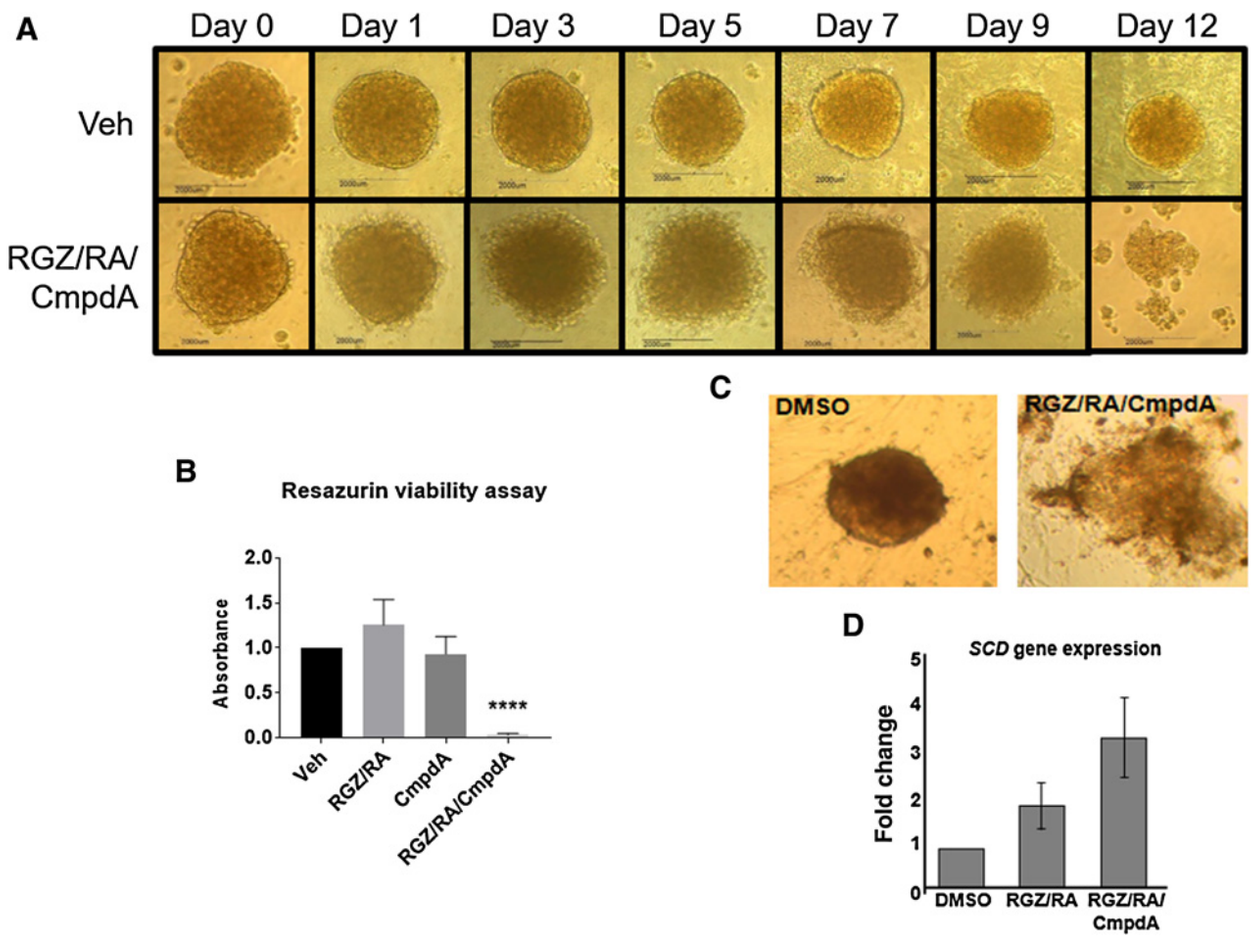

Figure 4.

Effects of combined PPARγ activation and XIAP inhibition in KGN spheroids (**A** and **B**) and GCT explant (**C** and **D**). Combination treatment (RGZ/RA/CmpdA) at the same concentrations used for the 2D monolayer experiments was used to treat KGN spheroids and GCT explant over 12- and 7-day period, respectively. Cell viability of the KGN spheroids was assessed using the resazurin viability assay (**B**). $n = 3$ in quadruplicate wells; one-way ANOVA; Tukey *post hoc* analysis; *, $P < 0.05$ when compared with vehicle (Veh; 0.1% DMSO). Representative of one GCT sample showing concomitant loss of cell viability after RGZ/RA/CmpdA treatment (**C**). Expression of a PPARγ-induced gene, *steraoyl-CoA desaturase 1* (*SCD*), was investigated after the combination treatment in the GCT explants (**D**). $n = 2$. Mean ± SD.

viability (Fig. 4C). We also measured the gene expression levels of stearoyl-CoA desaturase-1 (*SCD*), a PPARγ-induced gene that has been reported to be stimulated following RGZ treatment (28). *SCD* encodes the SCD protein that was highly induced after the combination treatment in KGN cells (D.T.H. Leung; unpublished observations). We observed that there was robust induction of *SCD* gene expression after the combination treatment in the explant samples (Fig. 4D), indicating that PPARγ is being activated by the combined treatment.

Combined XIAP inhibition and PPARγ activation delayed invasion

In advanced stage ovarian cancer, aggregates of cancer cells attach to and invade the peritoneal lining to promote metastasis. Utilizing the xCELLigence RTCA system, we investigate whether combined inhibition of XIAP and PPARγ activation can reduce the invasiveness of the KGN cells. We observed that RGZ/RA/CmpdA-treated KGN cells have a delayed onset of invasion by approximately 8 hours and were less invasive than vehicle-treated cells (Fig. 5A and B).

Combined XIAP inhibition and PPARγ activation decreases mitochondrial respiration and reduces spare respiratory capacity

We next explored the underlying mechanisms of the cytotoxic effect by the combination treatment. PPARγ plays a pivotal role in lipid and glucose metabolism, and there is upregulation of proteins associated with metabolic processes in combined treated GCT-derived cell lines, consistent with the restoration of PPARγ activity (D.T.H. Leung; unpublished observations). Given the pivotal role of mitochondria for energy metabolism in determining cell fate and the association of oxidative stress with the XIAP/Smac signaling pathway, we investigated whether the combined treatment would affect mitochondrial oxygen consumption in the KGN cells. We performed mitochondrial respiratory analysis using Extracellular Flux Analyzer (XFp) to determine

Published OnlineFirst December 7, 2018; DOI: 10.1158/1535-7163.MCT-18-0078

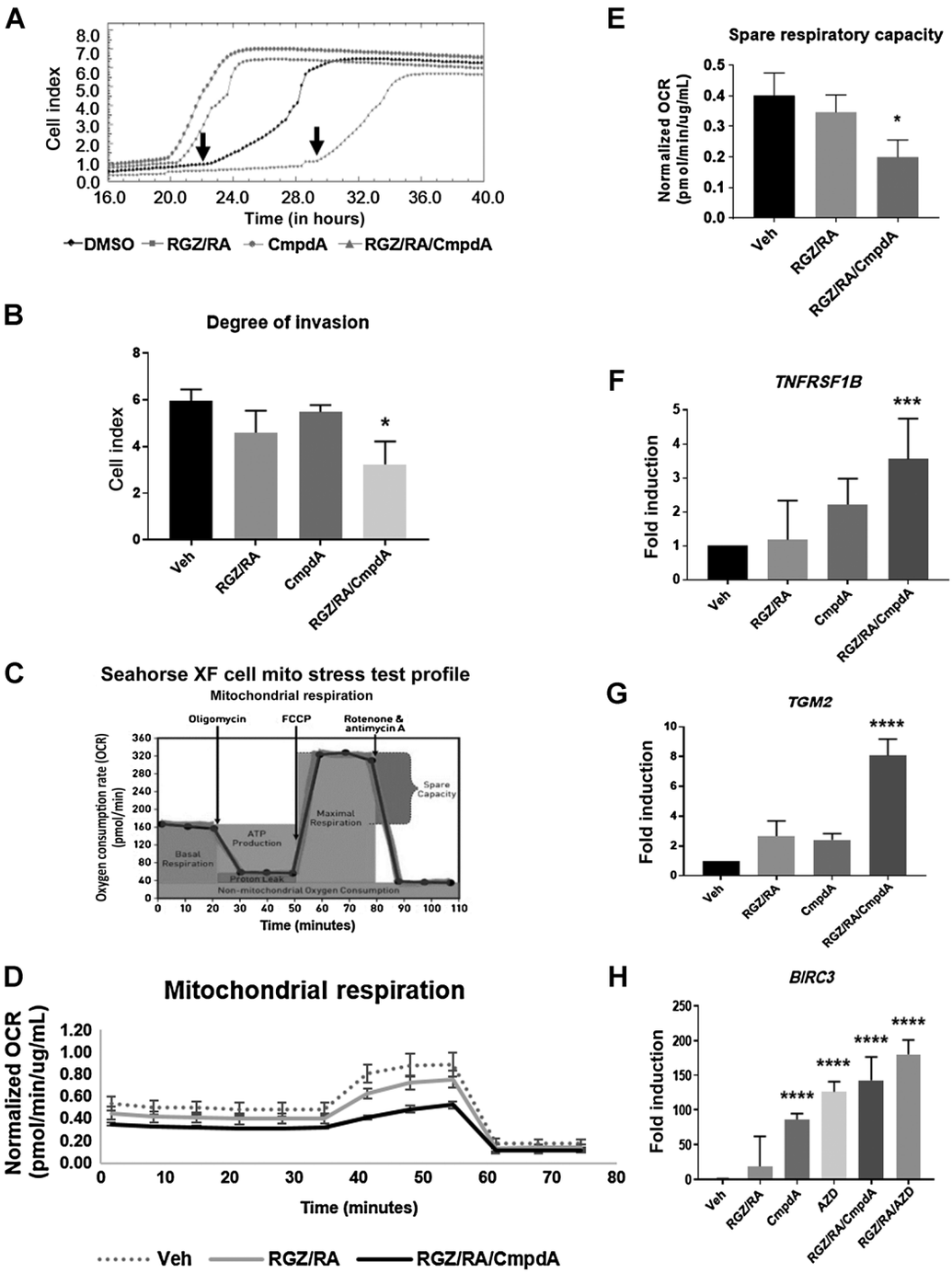

Figure 5.

Effects of combined PPARγ activation and XIAP inhibition in KGN. RGZ/RA (20 μmol/L/5 μmol/L) and CmpdA (500 nmol/L) was used alone or in combination to activate PPARγ and inhibit XIAP, respectively. **A** and **B,** Invasion assay. Onset of invasion (**A**, indicated by arrows, representative of 3 separate experiments) and overall invasiveness (**B**) in the treated cells compared with the vehicle (Veh; 0.1% DMSO) treatment. Mean ± SD. $n = 3$ in duplicate wells; one-way ANOVA; Tukey *post hoc* analysis; *, $P < 0.05$ when compared with vehicle. **C–E,** Seahorse extracellular flux assay in KGN. A schematic representation of the design and interpretation of the assay (**C**). Mitochondrial respiration (**D**), represented by the OCR, was measured as the control and treated KGN cells were subjected to metabolic stressors, oligomycin, FCCP, and antimycin A/rotenone. Spare respiratory capacity (**E**) represents the ability of the cells to respond to an increased energy demand. Mean ± SD. $n = 3$ in duplicate wells; one-way ANOVA; Tukey *post hoc* analysis; *, $P < 0.05$ when compared with vehicle. **F–H,** Gene expression analysis. mRNA levels of the proapoptotic genes, *TNFRSF1B* (**F**) and *TGM2* (**G**), were investigated using digital PCR following the combined PPARγ activation and XIAP inhibition (10 μmol/L Emb or 500 nmol/L CmpdA). **H,** Quantitative PCR showed changes of an IAP member, *cIAP2* or *BIRC3*, followed by the two Smac-mimetics, CmpdA and AZD (both at 500 nmol/L), alone or in combination with RGZ/RA. Mean ± SD. $n = 3$–7 in duplicate wells; Kruskal–Wallis; Dunn's *post hoc* analysis; *, $P < 0.05$; ***, $P < 0.001$; ****, $P < 0.0001$ when compared with vehicle (Veh; 0.1% DMSO).

Published OnlineFirst December 7, 2018; DOI: 10.1158/1535-7163.MCT-18-0078

whether the oxygen consumption rate (OCR) was altered by the combined treatment. A schematic representation of the design and interpretation of this assay is shown in Fig. 5C. OCR was measured every 9 minutes as multiple mitochondrial inhibitors including oligomycin, FCCP, and antimycin A/rotenone were added to the KGN cells in the presence or absence of the treatment. Although RGZ/RA caused a nonsignificant reduction in OCR over the time course of the experiment, the combined XIAP inhibition and PPARγ activation significantly decreased OCR (Fig. 5D). By measuring the spare respiratory capacity, which is an estimate of the potential bioenergetic reserve the cell can call upon in times of stress, we observed a significant reduction in the combined treated cells compared with vehicle- or RGZ/RA-treated cells (Fig. 5E). This indicates that the combined treatment affected mitochondrial function, inhibiting the ability of the mitochondria to function at their full potential, causing the reserve capacity to be significantly reduced.

TLDA analysis of XIAP inhibition and PPARγ activation in KGN cells

The expression of 93 apoptosis-related genes was analyzed using TaqMan Low Density Arrays (Supplementary Table S1). Relative gene expression was normalized against the median of geNorm software selected controls. Genes that showed the highest induction after the combined treatment compared with vehicle control were *TNFRSF1B* (TNF Receptor Superfamily Member 1B, 2.3-fold) and *BIRC3* (baculovirus IAP repeat-containing 3 or cIAP2, 139.8-fold).

The induction of these genes, together with *TGM2*, was validated using qRT-PCR. *TGM2* encodes the proapoptotic protein transglutaminase-2 (29), and we previously identified using a proteomic approach called the stable isotope labeling with amino acid in cell culture (SILAC) coupled with mass spectrometry, that the protein levels of TGM2 were upregulated by 2.3-fold after the RGZ/RA/CmpdA treatment in the KGN cells (D.T.H. Leung; unpublished observations). Cells were treated with DMSO (vehicle; 0.1%), PPARγ/RXRα agonists (RGZ/RA 20 μmol/L/5 μmol/L), Smac-mimetics (Cmpd A and AZD at 500 nmol/L, for BIRC3) alone and a combination of Smac-mimetics and PPARγ/RXRα agonists. Gene expression is presented as a change in fold induction, relative to *RPLP0* control and normalized to vehicle control. *TNFRSF1B* expression following RGZ/RA treatment alone was not significantly increased. However, *TNFRSF1B* was significantly upregulated following RGZ/RA/CmpdA treatment (Fig. 5F). We observed an 8-fold increase of *TGM2* mRNA levels after the combined treatment (Fig. 5G). For *BIRC3* mRNA levels, CmpdA and AZD treatments resulted in significantly increased induction when used alone or in combination with RGZ/RA. RGZ/RA treatment did not affect *BIRC3* mRNA levels (Fig. 5H).

Discussion

The molecular mechanisms of PPARγ action in ovarian function are poorly understood. PPARγ is antiproliferative, promoting terminal differentiation in GC and alterations in steroidogenesis (30). It is involved in GC atresia as activation of PPARγ induces apoptosis in primary rat GCs (30). PPARγ is implicated in the pathology of several diseases including obesity, diabetes, and polycystic ovarian syndrome (30). PPARγ agonist ligands, the synthetic thiazolidinediones (TZD), for example, troglitazone and rosiglitazone, have been developed to treat patients with type II diabetes (31). The potential of PPARγ agonists as anticancer agents has attracted considerable interest due to exerting antineoplastic effects in various solid tumors including endocrine malignancies (32–35). The prodifferentiating role of PPARγ is associated with inhibition of tumor development and progression (36). The overexpression of PPARγ in cancers such as the colon and thyroid allows these cancer cells to be targeted with PPARγ agonists and has led to *in vitro* studies with PPARγ agonists, which show a reduction in cell viability and inhibition of cell proliferation (37, 38). These antitumor effects have also been observed in xenograft models of solid tumors (39).

High levels of PPARγ in the GCT at the mRNA level (2) and subsequently in this study at the protein level were unexpected given the antiproliferative properties of PPARγ, suggesting that, although potentially targetable, there is resistance to its actions in GCT. Our findings that the TZDs alone have only a small effect on GCT cell proliferation and transactivation activity is consistent with this conclusion (Fig. 2A and B).

We have previously reported that another NR, the antiproliferative ERβ is also upregulated in the GCT-derived cell lines (6). However, ligand-associated ERβ signaling is inhibited by constitutive activation of NFκB signaling, GCT-derived cells transfected with estrogen-responsive reporter constructs showed no response when treated with estradiol (6). Similar, glucocorticoid receptor (GR)–mediated transactivation is also repressed by NFκB signaling in these cell lines (6). Inhibition of the NFκB pathway using the IκBα-specific inhibitor, BAY11-7082, restored both ER- and GR-mediated transactivation (6). These data demonstrated that the functional consequence of constitutive NFκB activity is the transrepression of ERβ-mediated transcription in the COV434 and KGN cell lines (6). Consistent with these published data, in this study, we demonstrated that the observed PPARγ resistance in the GCT-derived cells was also mediated by constitutive NFκB activity causing transrepression of PPARγ. With inactivation of NFκB signaling, PPARγ agonists led to a profound effect with decreased proliferation (Fig. 2A), increased apoptosis (Fig. 2C and D), and PPARγ-mediated transactivation at the PPRE resulting in a 5-fold induction in response to ligand (Fig. 2B).

Given their respective physiologic roles, mutual transrepression between NFκB and GR results in a cooperative modulation of inflammation and immunosuppression. However, the significance of constitutive activation of NFκB with consequent transrepression of PPARγ in the pathogenesis of GCT remains speculative. In addition to repressing the antiproliferative function of PPARγ in granulosa cells (30, 40), activation of NFκB signaling in GCT may also provide a survival advantage through increasing the expression of genes involved in cell proliferation, metastasis, angiogenesis, and antiapoptosis (3).

The IAPs are critical modulators of apoptosis as they inhibit activation (cIAP1/2) or activity of (XIAP) caspases, a process that initiates apoptosis. Among the 8-member IAP family, the best characterized and most potent caspase inhibitor, XIAP, is transcriptionally activated by NFκB. In addition, XIAP has a reciprocal modulatory role in NFκB activation as a consequence of a positive feed-forward loop. XIAP can activate the NFκB and AP1 signaling pathways involving the TAK–TAB protein complex via a physical interaction between XIAP BIR1 domain and the TGFβ-activated kinase-binding (TAB) protein 1 (26). We have demonstrated that NFκB and TGFβ coordinately regulate cell survival in GCT (41). It

Published OnlineFirst December 7, 2018; DOI: 10.1158/1535-7163.MCT-18-0078

remains to be determined whether the constitutive activity of both NFκB and AP1 (6, 42) in the GCT-derived cell lines is regulated through TAK–TAB complex.

XIAP is a critical regulator of follicular atresia (43). FSH induces XIAP expression, which in turn suppresses GC apoptosis to facilitate FSH-induced follicular cell expansion and development (43). XIAP is highly expressed in proliferating GC of gonadotropin-primed follicles and downregulated in apoptotic cells from atretic follicles after gonadotropin withdrawal (43). FSH induces XIAP expression in GC *in vitro* via the NFκB pathway (44). In this study, we showed that XIAP is overexpressed in our cohort of primary GCT and in KGN and COV434 cells, likely due to constitutive activation of the NFκB pathway.

Because of its elevated expression and prominent ability to control cell death in many human cancers, XIAP has become an attractive therapeutic target for novel anticancer treatment (11, 12). Smac-mimetics are small-molecule inhibitors designed to mimic the natural IAP antagonist Smac and bind directly to XIAP with high affinity to neutralize the pro-oncogenic functions of this protein, by preventing caspase binding (11, 12). Mono- or bivalent Smac-mimetics have been designed to target the BIR2 and/or BIR3 functional domains. Preclinical studies have reported high anti-neoplastic activity by both monovalent and bivalent compounds. Several of these compounds have also demonstrated favorable safety profiles and evidence of antitumor activity in early clinical trials (11, 12, 45). Although originally designed to inactivate XIAP, Smac-mimetics are also effective in producing rapid ubiquitylation and proteasomal degradation of other members of the IAP family, in particular cIAP1 and cIAP2 (46, 47).

We have shown that XIAP is the predominant IAP expressed in GCT and the levels of other members are low. In our studies, we utilized a bivalent Smac-mimetic, CmpdA (22), and a commercial monovalent compound, AZD5582. We demonstrated that these compounds have no effect on cell proliferation, PPARγ transactivation or apoptosis when used as a single treatment. However, we observed in cells transfected with either an NFκB or AP1 reporter, that inhibition of XIAP abrogated constitutive activity for both pathways (Fig. 3A and B), indicating that XIAP is regulating both pathways, potentially through the TAK1/TAB1/2/3 complex.

Inhibiting XIAP using single agents has shown some signs of antitumor activity; however, the majority of studies indicate a better efficacy can be achieved with combining drugs (11, 12). In this study, we presented strong evidence that PPARγ agonism in combination with inhibition of NFκB signaling (by XIAP inhibition) is a potential efficacious, molecular-targeted therapy for GCT treatment. XIAP is an attractive therapeutic target due to: (i) its inhibition of intrinsic antiapoptotic properties; (ii) its ability to block NFκB activation; and (iii) its relative tissue specificity. Our data show that this is the case for GCT-derived cell lines, in monolayer and 3D spheroids, which mimic the tumor microenvironment, and is also likely relevant for primary GCT given the similar effects on two *in vivo* GCT explants from patient tumor samples.

The role of PPARγ in adipogenesis and metabolic homeostasis led us to investigate the effect of the combined treatment on metabolic function by measuring mitochondrial respiration. Generation of ATP by mitochondrial respiration is an indispensable source of energy. Many cells and tissues operate at a basal level, only requiring a part of their total bioenergetic capability thus allowing a reserve respiratory capacity for sudden surges in energy requirement. We observed that the combined treatment reduced the available reserve respiratory capacity, indicating that the combined treatment sensitizes the GCT-derived cells to a sudden surge in ATP demand. However, as the reserve is depleted, it causes the cells to undergo cell death (Fig. 5D–E).

The evidence that XIAP and PPARγ cotreatment induces apoptosis and alters cellular bioenergetics is supported by the gene expression analysis where proapoptotic genes such as *TNFRSF1B*, *TGM2*, and *BIRC3* are found to be upregulated. In addition, we also identified from our proteomic study (D.T.H. Leung; unpublished observations), the downregulation of fascin, a protein associated with cell motility. Cell motility is another major challenge for GCT treatment as it contributes to the metastatic process of cancer cells by allowing cells to attach to and invade the peritoneal lining to form secondary tumors. In this study, we observed that the RGZ/RA/CmpdA-treated KGN cells when compared to vehicle, significantly delayed the onset and level of invasion. Proliferation of the RGZ/RA/CmpdA-treated cells ceased postinvasion, as represented by the plateau of the cell index (Fig. 5A). This may indicate the cells are undergoing differentiation due to PPARγ activity being restored. It also suggests that the combined treatment strategy may also be advantageous in preventing the metastatic process.

This study provides a proof of concept for combination therapeutic targeting involving XIAP inhibition and PPARγ activation for GCT. We anticipate this targeted therapy will contribute to reducing the use of broad nonspecific standard chemotherapy. As these drugs are already in clinical or preclinical use, expedient translation to the clinic is possible. The findings presented in this study may also have broader significance beyond GCT, specifically for malignancies that coexpress these proteins such as epithelial ovarian cancer (48, 49), colorectal cancer (50), and thyroid cancer (51, 52).

Disclosure of Potential Conflicts of Interest

No potential conflicts of interest were disclosed.

Authors' Contributions

Conception and design: S. Chu

Development of methodology: D.T.H. Leung, T. Nguyen, E.M. Oliver, J. Matti, J. Silke, S. Chu

Acquisition of data (provided animals, acquired and managed patients, provided facilities, etc.): D.T.H. Leung, T. Nguyen, E.M. Oliver, J. Matti, T.W. Jobling, S. Chu

Analysis and interpretation of data (e.g., statistical analysis, biostatistics, computational analysis): D.T.H. Leung, E.M. Oliver, J. Matti, P.J. Fuller, S. Chu

Writing, review, and/or revision of the manuscript: D.T.H. Leung, T. Nguyen, M. Alexiadis, P.J. Fuller, S. Chu

Administrative, technical, or material support (i.e., reporting or organizing data, constructing databases): D.T.H. Leung, T. Nguyen, J. Silke, T.W. Jobling, S. Chu

Study supervision: P.J. Fuller, S. Chu

Acknowledgments

This work was supported by grants-in-aid from the Cancer Council Victoria (to P.J. Fuller and S. Chu), the Ovarian Cancer Research Foundation (to S. Chu), the Granulosa Cell Tumour of the Ovary Foundation (to S. Chu and P.J. Fuller), the Marsha Rivkin Center for Ovarian Cancer Research (to S. Chu and P.J. Fuller), the National Health & Medical Research Council of Australia through a Project Grant (#1058334; to P.J. Fuller and S. Chu), Ian Potter Foundation for the Seahorse Extracellular Flux XFp Analyzer (to S. Chu), and Endocrine Society of Australia through a Research Higher Degree Scholarship (to D.T.H. Leung). The Hudson Institute is supported by the Victorian Government's Operational Infrastructure Scheme. The authors thank Calvin Chee (Hudson Institute of Medical Research), Nicholas Chee (Hudson Institute of

Medical Research), Daniel Heathcote (Hudson Institute of Medical Research), and the MHTP Research Platforms for technical support. We would also like to thank Professor Akira Iwase (Nagoya University Graduate School of Medicine) for kindly providing the hGrC1 cell line (18). We would like to acknowledge MHTP medical Genomics Facility, Melbourne, Australia, as the service provider for quantitative PCR and high content screening.

The costs of publication of this article were defrayed in part by the payment of page charges. This article must therefore be hereby marked *advertisement* in accordance with 18 U.S.C. Section 1734 solely to indicate this fact.

Received January 22, 2018; revised June 25, 2018; accepted December 4, 2018; published first December 7, 2018.

References

1. Jamieson S, Fuller PJ. Molecular pathogenesis of granulosa cell tumors of the ovary. Endocr Rev 2012;33:109–44.
2. Alexiadis M, Eriksson N, Jamieson S, Davis M, Drummond AE, Chu S, et al. Nuclear receptor profiling of ovarian granulosa cell tumors. Hormones Cancer 2011;2:157–69.
3. Baldwin AS. Regulation of cell death and autophagy by IKK and NF-kappaB: critical mechanisms in immune function and cancer. Immunol Rev 2012;246:327–45.
4. Baldwin AS Jr.The NF-kappa B and I kappa B proteins: new discoveries and insights. Annu Rev Immunol 1996;14:649–83.
5. Karin M, Cao Y, Greten FR, Li ZW. NF-kappaB in cancer: from innocent bystander to major culprit. Nat Rev Cancer 2002;2:301–10.
6. Chu S, Nishi Y, Yanase T, Nawata H, Fuller PJ. Transrepression of estrogen receptor beta signaling by nuclear factor-kappab in ovarian granulosa cells. Mol Endocrinol 2004;18:1919–28.
7. McKay LI, Cidlowski JA. Molecular control of immune/inflammatory responses: interactions between nuclear factor-kappa B and steroid receptor-signaling pathways. Endocr Rev 1999;20:435–59.
8. Vaux DL, Silke J. IAPs, RINGs and ubiquitylation. Nat Rev Mol Cell Biol 2005;6:287–97.
9. Du C, Fang M, Li Y, Li L, Wang X. Smac, a mitochondrial protein that promotes cytochrome c-dependent caspase activation by eliminating IAP inhibition. Cell 2000;102:33–42.
10. Verhagen AM, Ekert PG, Pakusch M, Silke J, Connolly LM, Reid GE, et al. Identification of DIABLO, a mammalian protein that promotes apoptosis by binding to and antagonizing IAP proteins. Cell 2000;102:43–53.
11. Fulda S. Smac mimetics to therapeutically target IAP proteins in cancer. Int Rev Cell Mol Biol 2017;330:157–69.
12. Fulda S. Promises and challenges of smac mimetics as cancer therapeutics. Clin Cancer Res 2015;21:5030–6.
13. Jamieson S, Butzow R, Andersson N, Alexiadis M, Unkila-Kallio L, Heikinheimo M, et al. The FOXL2 C134W mutation is characteristic of adult granulosa cell tumors of the ovary. Mod Pathol 2010;23:1477–85.
14. Alexiadis M, Chu S, Leung D, Gould JA, Jobling T, Fuller PJ. Transcriptomic analysis of stage 1 versus advanced adult granulosa cell tumors. Oncotarget 2016;7:14207–19.
15. Jamieson S, Fuller PJ. Characterization of the inhibitor of kappaB kinase (IKK) complex in granulosa cell tumors of the ovary and granulosa cell tumor-derived cell lines. Horm Cancer 2013;4:277–92.
16. Nishi Y, Yanase T, Mu Y, Oba K, Ichino I, Saito M, et al. Establishment and characterization of a steroidogenic human granulosa-like tumor cell line, KGN, that expresses functional follicle-stimulating hormone receptor. Endocrinology 2001;142:437–45.
17. van den Berg-Bakker CA, Hagemeijer A, Franken-Postma EM, Smit VT, Kuppen PJ, van Ravenswaay Claasen HH, et al. Establishment and characterization of 7 ovarian carcinoma cell lines and one granulosa tumor cell line: growth features and cytogenetics. Int J Cancer 1993;53:613–20.
18. Bayasula IA, Kiyono T, Takikawa S, Goto M, Nakamura T, et al. Establishment of a human nonluteinized granulosa cell line that transitions from the gonadotropin-independent to the gonadotropin-dependent status. Endocrinology 2012;153:2851–60.
19. Handeli S, Simon JA. A small-molecule inhibitor of Tcf/beta-catenin signaling down-regulates PPARgamma and PPARdelta activities. Mol Cancer Ther 2008;7:521–9.
20. Lee J, Rhee MH, Kim E, Cho JY. BAY 11–7082 is a broad-spectrum inhibitor with anti-inflammatory activity against multiple targets. Mediators Inflamm 2012;2012:416036.
21. Kim SK, Abdelmegeed MA, Novak RF. The mitogen-activated protein kinase kinase (mek) inhibitor PD98059 elevates primary cultured rat hepatocyte glutathione levels independent of inhibiting mek. Drug Metab Dispos 2006;34:683–9.
22. Vince JE, Wong WW, Khan N, Feltham R, Chau D, Ahmed AU, et al. IAP antagonists target cIAP1 to induce TNFalpha-dependent apoptosis. Cell 2007;131:682–93.
23. Hennessy EJ, Adam A, Aquila BM, Castriotta LM, Cook D, Hattersley M, et al. Discovery of a novel class of dimeric Smac mimetics as potent IAP antagonists resulting in a clinical candidate for the treatment of cancer (AZD5582). J Med Chem 2013;56:9897–919.
24. Nikolovska-Coleska Z, Xu L, Hu Z, Tomita Y, Li P, Roller PP, et al. Discovery of embelin as a cell-permeable, small-molecular weight inhibitor of XIAP through structure-based computational screening of a traditional herbal medicine three-dimensional structure database. J Med Chem 2004;47:2430–40.
25. Bilandzic M, Stenvers KL. Assessment of ovarian cancer spheroid attachment and invasion of mesothelial cells in real time. J Vis Exp 2014.
26. Lu M, Lin SC, Huang Y, Kang YJ, Rich R, Lo YC, et al. XIAP induces NF-kappaB activation via the BIR1/TAB1 interaction and BIR1 dimerization. Mol Cell 2007;26:689–702.
27. Resch U, Schichl YM, Winsauer G, Gudi R, Prasad K, de Martin R. Siva1 is a XIAP-interacting protein that balances NFkappaB and JNK signalling to promote apoptosis. J Cell Sci 2009;122:2651–61.
28. Kolak M, Yki-Jarvinen H, Kannisto K, Tiikkainen M, Hamsten A, Eriksson P, et al. Effects of chronic rosiglitazone therapy on gene expression in human adipose tissue in vivo in patients with type 2 diabetes. J Clin Endocrinol Metab 2007;92:720–4.
29. Roszer T. Transcriptional control of apoptotic cell clearance by macrophage nuclear receptors. Apoptosis 2017;22:284–94.
30. Froment P, Gizard F, Defever D, Staels B, Dupont J, Monget P. Peroxisome proliferator-activated receptors in reproductive tissues: from gametogenesis to parturition. J Endocrinol 2006;189:199–209.
31. Aleman-Gonzalez-Duhart D, Tamay-Cach F, Alvarez-Almazan S, Mendieta-Wejebe JE. Current advances in the biochemical and physiological aspects of the treatment of type 2 diabetes mellitus with thiazolidinediones. PPAR Res 2016;2016:7614270.
32. Smallridge RC, Copland JA, Brose MS, Wadsworth JT, Houvras Y, Menefee ME, et al. Efatutazone, an oral PPAR-gamma agonist, in combination with paclitaxel in anaplastic thyroid cancer: results of a multicenter phase 1 trial. J Clin Endocrinol Metab 2013;98:2392–400.
33. Komatsu Y, Yoshino T, Yamazaki K, Yuki S, Machida N, Sasaki T, et al. Phase 1 study of efatutazone, a novel oral peroxisome proliferator-activated receptor gamma agonist, in combination with FOLFIRI as second-line therapy in patients with metastatic colorectal cancer. Invest New Drugs 2014;32:473–80.
34. Murakami H, Ono A, Takahashi T, Onozawa Y, Tsushima T, Yamazaki K, et al. Phase I study of efatutazone, an oral PPARgamma agonist, in patients with metastatic solid tumors. Anticancer Res 2014;34:5133–41.
35. Catalano MG, Poli R, Pugliese M, Fortunati N, Boccuzzi G. Emerging molecular therapies of advanced thyroid cancer. Mol Aspects Med 2010;31:215–26.
36. Ferrari SM, Materazzi G, Baldini E, Ulisse S, Miccoli P, Antonelli A, et al. Antineoplastic effects of PPARgamma agonists, with a special focus on thyroid cancer. Curr Med Chem 2016;23:636–49.
37. Tsukahara T. The role of PPARgamma in the transcriptional control by agonists and antagonists. PPAR Res 2012;2012:362361.
38. Antonelli A, Fallahi P, Ulisse S, Ferrari SM, Minuto M, Saraceno G, et al. New targeted therapies for anaplastic thyroid cancer. Anticancer Agents Med Chem 2012;12:87–93.
39. Shimazaki N, Togashi N, Hanai M, Isoyama T, Wada K, Fujita T, et al. Antitumour activity of CS-7017, a selective peroxisome proliferator-activated receptor gamma agonist of thiazolidinedione class, in human tumour xenografts and a syngeneic tumour implant model. Eur J Cancer 2008;44:1734–43.

40. Komar CM. Peroxisome proliferator-activated receptors (PPARs) and ovarian function–implications for regulating steroidogenesis, differentiation, and tissue remodeling. Reprod Biol Endocrinol 2005;3:41.
41. Bilandzic M, Chu S, Wang Y, Tan HL, Fuller PJ, Findlay JK, et al. Betaglycan alters NFkappaB-TGFbeta2 cross talk to reduce survival of human granulosa tumor cells. Mol Endocrinol 2013;27:466–79.
42. Chu S, Alexiadis M, Fuller PJ. Proteasome inhibition by bortezomib decreases proliferation and increases apoptosis in ovarian granulosa cell tumors. Reprod Sci 2009;16:397–407.
43. Wang Y, Rippstein PU, Tsang BK. Role and gonadotrophic regulation of X-linked inhibitor of apoptosis protein expression during rat ovarian follicular development in vitro. Biol Reprod 2003;68:610–9.
44. Wang Y, Chan S, Tsang BK. Involvement of inhibitory nuclear factor-kappaB (NFkappaB)-independent NFkappaB activation in the gonadotropic regulation of X-linked inhibitor of apoptosis expression during ovarian follicular development in vitro. Endocrinology 2002;143: 2732–40.
45. Condon SM, Mitsuuchi Y, Deng Y, LaPorte MG, Rippin SR, Haimowitz T, et al. Birinapant, a smac-mimetic with improved tolerability for the treatment of solid tumors and hematological malignancies. J Med Chem 2014;57:3666–77.
46. Darding M, Feltham R, Tenev T, Bianchi K, Benetatos C, Silke J, et al. Molecular determinants of Smac mimetic induced degradation of cIAP1 and cIAP2. Cell Death Differ 2011;18:1376–86.
47. Feltham R, Bettjeman B, Budhidarmo R, Mace PD, Shirley S, Condon SM, et al. Smac mimetics activate the E3 ligase activity of cIAP1 protein by promoting RING domain dimerization. J Biol Chem 2011;286:17015–28.
48. Zhang GY, Ahmed N, Riley C, Oliva K, Barker G, Quinn MA, et al. Enhanced expression of peroxisome proliferator-activated receptor gamma in epithelial ovarian carcinoma. Br J Cancer 2005;92:113–9.
49. Wu M, Yuan S, Szporn AH, Gan L, Shtilbans V, Burstein DE. Immunocytochemical detection of XIAP in body cavity effusions and washes. Mod Pathol 2005;18:1618–22.
50. Qiao L, Dai Y, Gu Q, Chan KW, Ma J, Lan HY, et al. Loss of XIAP sensitizes colon cancer cells to PPARgamma independent antitumor effects of troglitazone and 15-PGJ2. Cancer Lett 2008;268:260–71.
51. Zhang Y, Yu J, Lee C, Xu B, Sartor MA, Koenig RJ. Genomic binding and regulation of gene expression by the thyroid carcinoma-associated PAX8-PPARG fusion protein. Oncotarget 2015;6:40418–32.
52. Hussain AR, Bu R, Ahmed M, Jehan Z, Beg S, Al-Sobhi S, et al. Role of X-Linked inhibitor of apoptosis as a prognostic marker and therapeutic target in papillary thyroid carcinoma. J Clin Endocrinol Metab 2015; 100:E974–85.

Journal of proteome research

Article

Cite This: J. Proteome Res. 2019, 18, 1691−1702

pubs.acs.org/jpr

Targeting XIAP and PPARγ in Granulosa Cell Tumors Alters Metabolic Signaling

Dilys T. H. Leung,[†,§] Adam Rainczuk,[†] Trang Nguyen,[†] Andrew Stephens,[†] John Silke,[‡] Peter J. Fuller,[†] and Simon Chu*[,†]

[†]Department of Molecular and Translational Science, Hudson Institute of Medical Research and the Monash University, Clayton, Victoria 3168, Australia

[‡]Walter and Eliza Hall Institute of Medical Research, Parkville, Victoria 3052, Australia

Supporting Information

ABSTRACT: Ovarian granulosa cell tumors (GCTs) are hormonally active cancers characterized by indolent growth and late, invasive relapse. No therapies have yet proven to be efficacious. We previously reported that the inhibition of the antiapoptotic X-linked inhibitor of apoptosis protein (XIAP) removes transrepression of the pro-proliferative nuclear receptor, peroxisome proliferator-activated receptor (PPAR)-γ, in a GCT-derived cell line, KGN. Both PPARγ and XIAP are overexpressed in human GCT. The inhibition of XIAP with the restoration of PPARγ signaling using a SMAC-mimetic (Compound A (CmpdA)) and rosiglitazone (RGZ)/retinoic acid (RA), respectively, reduced cell proliferation and induced apoptosis in the KGN cells. Utilizing stable isotope labeling with amino acids in cell culture, we identified 32 differentially expressed proteins in the KGN cells following the CmpdA/RGZ/RA-treatment, 22 of which were upregulated by ≥1.5 fold. Of these, stearoyl-CoA desaturase (SCD; 4.5-fold induction) was examined for putative binding sites for PPARγ using in silico screening. Chromatin immunoprecipitation confirmed the direct binding of PPARγ on the promoter region of *SCD*, with increased binding in the CmpdA/RGZ/RA-treated KGN cells. Because PPARγ plays a pivotal role in lipid and glucose metabolism, the upregulation of proteins associated with metabolic processes such as SCD is consistent with the restoration of PPARγ activity.

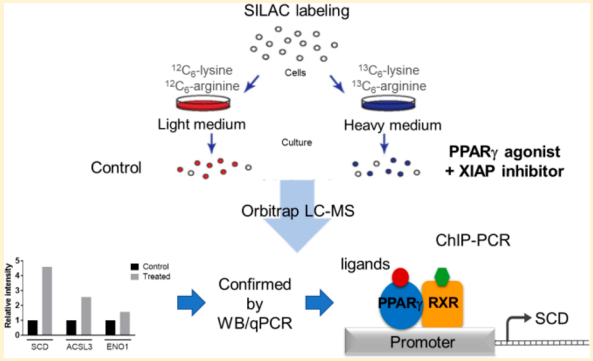

KEYWORDS: *apoptosis, granulosa cell tumors, ovary, proteomics, receptor binding*

INTRODUCTION

Granulosa cell tumors (GCTs) of the ovary are the most common type of ovarian sex cord-stromal tumors, which contribute ∼5% of all ovarian cancers.[1,2] The predominant adult GCT subtype (up to 95% compared with juvenile GCT) is defined by a single somatic FOXL2 C134W mutation.[1] The incidence of these tumors peaks between 50 and 54 years. Patients who present with FIGO stage-I disease have a relatively good prognosis. However, those who present with stage-III/IV disease have a 5 year survival rate of no greater than 50%.[1] GCTs are characterized by indolent growth and often relapse in aggressive form many years after primary treatment. Hormonal, chemo-, or radiotherapies have had limited efficacy; they are generally based on the regimen used for the treatment of the more common epithelial ovarian cancer, which despite a shared "organ of origin", is a separate disease.[2]

We have used the human adult GCT-derived cell line, KGN, to identify potential therapeutic targets for the treatment of these cancers. The KGN cell line was established from a recurrent metastatic GCT.[3] It harbors the FOXL2 C134W mutation that is pathognomonic for adult GCT.[4] We have previously shown using the KGN cell line that the X-linked inhibitor of apoptosis protein (XIAP) and the peroxisome proliferator-activated receptor (PPAR)-γ are potential therapeutic targets.[5] Both proteins are abundantly expressed in GCT.[6,7] PPARγ is well known for its involvement in lipid and glucose metabolism.[8] The thiazolidinediones (TZDs) are a class of PPARγ agonists that include rosiglitazone (RGZ) or pioglitazone, which have been used clinically as antidiabetic drugs.[8] In the ovary, PPARγ is expressed in granulosa cells (GCs) of developing follicles.[9] It promotes terminal differentiation,[10] inhibits proliferation, and induces apoptosis in rat GC and primary GC.[10,11] Overexpression of PPARγ is seen in many tumor types, for example, thyroid[12] and colon[13] cancers. Given the involvement of PPARγ in apoptosis and differentiation, the antitumor effects of TZDs have been investigated in various solid tumors.[14−16] The abundant expression of PPARγ in GCT, despite its obvious antineoplastic effects,

Received: December 10, 2018
Published: February 1, 2019

DOI: 10.1021/acs.jproteome.8b00917
J. Proteome Res. 2019, 18, 1691−1702

appears paradoxical. In the KGN cell line, we have shown that constitutively activated nuclear factor-κB (NF-κB) signaling[17] upregulates its effector protein, the antiapoptotic XIAP, as well as transrepresses the pro-differentiation transcription factor, PPARγ.[5] Our study found that by combining a specific inhibitor of NF-κB, BAY11-7082, with RGZ (and retinoic acid (RA) to activate RXRα, the obligate heterodimeric partner of PPARγ), PPARγ signaling was enabled in the GCT cells.

XIAP is the most potent member of the Inhibitor of Apoptosis Protein (IAP) family. It physically interacts with caspase-3 and -7 via the linker region between the Baculoviral IAP Repeat (BIR) 1 and 2 domains as well as caspase-9 via the BIR3 domain to inhibit both intrinsic and extrinsic apoptotic pathways.[18] It is ubiquitously expressed and is upregulated by NF-κB signaling. In the ovary, XIAP is highly expressed in healthy follicles[19] and protects rat GC from apoptosis in vitro[20] and in vivo.[21] XIAP has been implicated in malignancies including ovarian,[22] pancreatic,[23] nasopharyngeal,[24] and acute myeloid leukemia.[25] Endogenous XIAP is inhibited by the mitochondrial protein, second mitochondrial-derived activator of caspases (SMACs). It binds and blocks the BIR2 and BIR3 domains of XIAP to inhibit their caspase-binding activity.[26,27] SMAC-mimetics are synthetic analogues of the endogenous SMAC that are currently in clinical trials for various cancers.[28,29] Other small-molecule inhibitors have been designed to block IAP binding to caspases. This approach leads to the induction of apoptosis and sensitizing of malignant cell lines to chemotherapy.[27,30]

In the ovary, XIAP is regulated by follicle-stimulating hormone (FSH) and NF-κB.[31] We have identified the involvement of XIAP in a feed-forward loop that contributes to the constitutive NF-κB activity in GCT cells.[5] Given the regulatory role of XIAP in NF-κB signaling, we used a SMAC-mimetic, Compound A (CmpdA),[32] to inhibit XIAP and remove the NF-κB transrepression of PPARγ. By combining XIAP inhibition (CmpdA) with PPARγ activation (RGZ and RA), we observed the significant induction of apoptosis, a significant reduction in cell viability, and proliferation in the KGN cell line. In this study, we have used stable isotope labeling with amino acids in cell culture (SILAC) to identify differentially expressed proteins after combined XIAP inhibition and PPARγ activation of the KGN cells.

EXPERIMENTAL METHODS

Cell Culture and Stable Isotope Labeling with Amino Acids in Cell Culture

The human GCT-derived cell line, KGN, was established as previously described.[3] The cells were cultured in SILAC DMEM:F12, as described below, in a 37 °C humidified incubator with 5% CO_2.

For labeling, DMEM:F12 was first supplemented with 10% dialyzed fetal bovine serum (FBS), 1% penicillin/streptomycin, and 2.4% HEPES buffer. The medium was supplemented with either ^{13}C6-^{15}N4-arginine (*Arg-10*) and ^{13}C6-^{15}N2-lysine (*Lys-8*) or the naturally occurring ^{12}C6-arginine and -lysine to produce heavy or light SILAC medium, respectively. After five passages, the incorporation of heavy or light amino acids (>95%) was confirmed using mass spectrometry.

Drug Treatments

All treatments were performed in media containing 2% dialyzed FBS. Compounds used include RGZ (20 μm) and RA (5 μm) in combination with CmpdA (500 nm) or embelin (Emb; 20 μm). Embelin is a cell-permeable, small-molecular-weight inhibitor of XIAP,[33] which was used to provide complementary and confirmatory data to show that antagonism of XIAP is required for the maximal response to PPARγ agonism. RGZ, RA, and Emb were purchased from Sigma-Aldrich (St. Louis, MO); CmpdA was supplied through Prof. John Silke, Walter and Eliza Hall Institute, Melbourne, Australia. "Light" cells were used as the vehicle control with 0.1% DMSO (Sigma-Aldrich), whereas "heavy" cells were treated with the compounds listed above. A reciprocal experiment was performed where "heavy" cells were the control and "light" cells were treated with the compounds. After 24 h of treatment, the cells were lysed with Universal Immunoprecipitation (UIP) lysis buffer (50 mM Trizma base, 150 mM NaCl, 2 mM EDTA, 2 mM EGTA, 25 mM NaF, 0.2% Triton X-100, 0.3% Nonidet P-40, and 25 mM β-glycerolphosphate) and protease inhibitor cocktail tablet (Roche Applied Science, Penzberg, Germany; 1 tablet per 10 mL of UIP lysis buffer). The lysates were precipitated using acetone to remove undesirable substances that may interfere with downstream analyses. Following incubation with acetone for 60 min at −20 °C, the proteins were pelleted by centrifugation, and the supernatant was removed.

Sample Preparation

Acetone-precipitated protein pellets were kept at −80 °C until processed. All centrifugation was performed at 14 000*g*. Each pellet was resuspended in 7 M urea and incubated in a sonicating water bath. 15 μg of each sample was mixed with 7 M urea, added to spin column, and centrifuged for 15 min; the flow-through was discarded. 100 μL of 20 mM dithiothreitol was added to each spin column and centrifuged for 10 min, and the flow-through was discarded. This was followed by the addition of 100 μL of 55 mM iodoactamide in 7 M urea with 20 min of incubation and 10 min of centrifugation. After discarding the flow-through, 100 μL of 7 M urea was added to a Vivacon 500 spin column (10 kDa molecular weight cutoff; Sartorius Stedium Biotech, Goettingen, Germany) and centrifuged for 15 min; this step was repeated three times. Next, 100 μL of 50 mM ammonium bicarbonate was added and centrifuged for 15 min three times. For digestion, trypsin solution (Promega, Madison, WI; enzyme to protein ratio = 1:50) was added to each column filter and incubated overnight at 37 °C. The digested peptides were centrifuged for 10 min, and the flow-through was collected. 50 μL of 1% formic acid (FA), then 100 μL of 1% FA were added to the column filter, each followed by centrifugation for 10 min. The peptide extracts were lyophilized by vacuum centrifugation to ∼2 μL and then resuspended with 0.1% trifluoroacetic acid in 2% acetonitrile (ACN) to a total volume of 100 μL.

Liquid Chromatography–Electrospray Ionization Tandem Mass Spectrometry

5 μL (15 μg) of each peptide sample was separated on a HPLC system (Thermo Fisher Scientific, Berman, Germany) using a separation column (Acclaim PepMap RSLC, C18, pore size 100 Å, particle size 2 μm, 75 μm inner diameter ×15 cm length; Thermo Fisher Scientific) and a trapping column (Acclaim PepMap100, C18, pore size 100 Å, particle size 3 μm, 75 μm ID × 2 cm length; Thermo Fisher Scientific). The HPLC system was coupled to an LTQ Orbitrap XL mass spectrometer (Thermo Fisher Scientific) using the following buffer system: (A) 2% ACN, 0.1% FA in water; (B) 80% ACN, 0.1% FA in water. For direct injection into the mass

DOI: 10.1021/acs.jproteome.8b00917
J. Proteome Res. 2019, 18, 1691−1702

spectrometer, 1 μL of the digests was loaded onto the trap column and washed for 5 min with 100% A at a flow rate 5 μL/min. Peptides were eluted at a 300 nL/min flow rate with the following 100 min gradient: 4% B for 10 min, gradient to 40% B over 50 min, gradient to 90% B in 20 min, 90% B for 10 min, gradient from 90 to 4% B in 30 s, and 4% B for 19.5 min. The LTQ Orbitrap XL instrument was operated in data-dependent mode to automatically switch between full-scan MS and MS/MS acquisition. Instrument control was through Thermo Tune Plus and Xcalibur software (Thermo Fisher Scientific).

Full-scan MS spectra (m/z = 300−1700) were acquired in the Orbitrap analyzer with resolution in the Orbitrap system set to r = 60 000. The standard mass spectrometric conditions for all experiments were: spray voltage, 1.25 kV; no sheath and auxiliary gas flow; heated capillary temperature, 200 °C; predictive automatic gain control enabled, and an S-lens radio frequency level of 50−60%. All unassigned charge states and charge state of one were rejected. The six most intense peptide ions with charge states ≥2 and minimum signal intensity of 1000 were sequentially isolated and fragmented in the high-pressure linear ion trap by low-energy collision-induced dissociation. An activation q = 0.25, activation time of 30 ms, and normalized collision energy of 35% were used. The resulting fragment ions were scanned out in the low-pressure ion trap at the "normal scan rate" (33,333 amu/s) and recorded with the secondary electron multipliers.

Data Analysis

Raw data were processed with MaxQuant software (version 2.3.02) and its built-in Andromeda search engine using the following parameter settings: trypsin as enzyme with two missed cleavages allowed, *Homo sapiens* as organism, oxidation (M) as variable modification, carbamidomethylation (C) as a fixed modification, 10 ppm MS tolerance, 0.8 Da fragment mass tolerance, and peptide and protein false discovery rates both at 1% (P < 0.05 significance threshold). The peak lists were searched against the Swiss-Prot database (version 2014_02).

Protein ratio quantification was adjusted for lysine/arginine labeling bias, and a normalized ratio was calculated for each protein within each sample. Proteins that were identified in both reciprocal experiments and differentially expressed by ≥1.5-fold were retained. At least one unique peptide must be identified for any protein to be included in further analyses. Protein ratios from the reciprocal experiments were averaged to calculate the final fold change. The mass spectrometry proteomics data have been deposited to the ProteomeXchange Consortium via the PRIDE[34] partner repository with the data set identifier PXD012509.

Construction of Protein−Protein Interaction Network and Functional Annotation Analysis

Regulated proteins were subjected to association analysis using the STRING database (Search Tool for the Retrieval of Interacting Genes/Proteins version 10[35]) to build a protein−protein interaction network. Identification of the over- or under-represented Gene Ontology (GO) biological processes was performed using GO Enrichment Analysis (http://geneontology.org/).[36]

SDS-PAGE and Western Blot Analysis

For Western blot analysis, 50 μg of total protein was separated by SDS-PAGE gel (10% resolving and 5% stacking). Proteins were transferred to a PDVF membrane using the Bio-Rad Mini Trans-Blot electrophoretic transfer system at 4 °C overnight. The membrane was blocked for 1 h at room temperature with TBS (50 mM Tris-HCl, 150 mM NaCl; pH 7.6) containing 5% BSA (Roche Applied Science). Incubation with mouse monoclonal anti-SCD1 antibody (1:1000; Abcam, Cambridge, U.K.) in 1% TBST (TBS with 1% Tween 20) was performed at 4 °C overnight with gentle rocking. Subsequently, the membrane was incubated with goat antimouse horseradish peroxidase-conjugated secondary antibody (1:4000; Dako, Agilent Technologies, Santa Clara, CA) for 2 h at room temperature. Proteins were detected by applying Amersham ECL Prime Western Blotting Detection Reagent (GE Healthcare, Little Chalfont, U.K.). The membrane was imaged and quantified using the Bio-Rad ChemiDoc XRS+ System and Image Lab version 4.1 (Bio-Rad, Hercules, CA).

Digital PCR Fluidigm Biomark HD System

RNA was extracted from the KGN cells following drug treatments with DMSO, RGZ/RA, CmpdA, or Emb alone, CmpdA/RGZ/RA, or Emb/RGZ/RA. The integrity of the RNA was assessed using an Agilent 2100 Bioanalyzer at the Single Cell Genomic Centre, Monash Health Translation Precinct, Melbourne, Australia. All RNA samples have a 260:280 ratio of between 1.5 and 1.8, and an RNA integrity number (RIN) of >9.500 of RNA was used for cDNA synthesis with SuperScript III reverse transcriptase (Invitrogen, Thermo Fisher Scientific, Waltham, MA). The RIN algorithm ranks the quality of RNA based on the presence or absence of degradation products on a scale of 1 to 10, where level-10 RNA is completely intact. For gene expression analysis using the Fluidigm Biomark HDSystem, all cDNA was preamplified to increase the number of copies of each gene to detectable levels as per Fluidigm Gene Expression Specific Target Amplification Quick Reference PN 68000133 RevC. 45 genes were selected based on several proteins identified from the SILAC study as well as genes that are involved in apoptosis, cell cycle, and steroidogenesis. 48 Taqman gene expression assays and 48 samples including three housekeeping genes and two negative controls were combined in a 48.48 Dynamic array IFC according to Fluidigm 48.48 Real-Time PCR Workflow Quick Reference PN 6800088. Data were analyzed using the Fluidigm Real-Time PCR Analysis software version 4.1.2.

Screening for Putative Binding Sites

We screened a region of 10kb upstream of the *SCD* transcriptional start site (www.ensembl.org/index.html) for PPARγ binding using the JASPAR data set (http://jaspar.genereg.net/; relative profile score threshold 80%).[37] Primers were designed to amplify regions capturing the putative binding sites to confirm binding following chromatin immunoprecipitation (ChIP).

Chromatin Preparation

2×10^7 KGN cells were plated on 150 mm dish. Cell viability of >90% was confirmed using the Countess automated cell counter (Thermo Fisher Scientific). The KGN cells were subjected to DMSO (0.1%), RGZ/RA (20 μM/5 μM), or CmpdA/RGZ/RA (500 nM/20 μM/5 μM) for 6 h. Chromatin was cross-linked using 1% formaldehyde added directly to the cells, mixed gently, and incubated at room temperature for 10 min. The cross-linking reaction was quenched by glycine at a final concentration of 0.125 M. Cells were washed with an equal volume of cold (4 °C) PBS

DOI: 10.1021/acs.jproteome.8b00917
J. Proteome Res. 2019, 18, 1691−1702

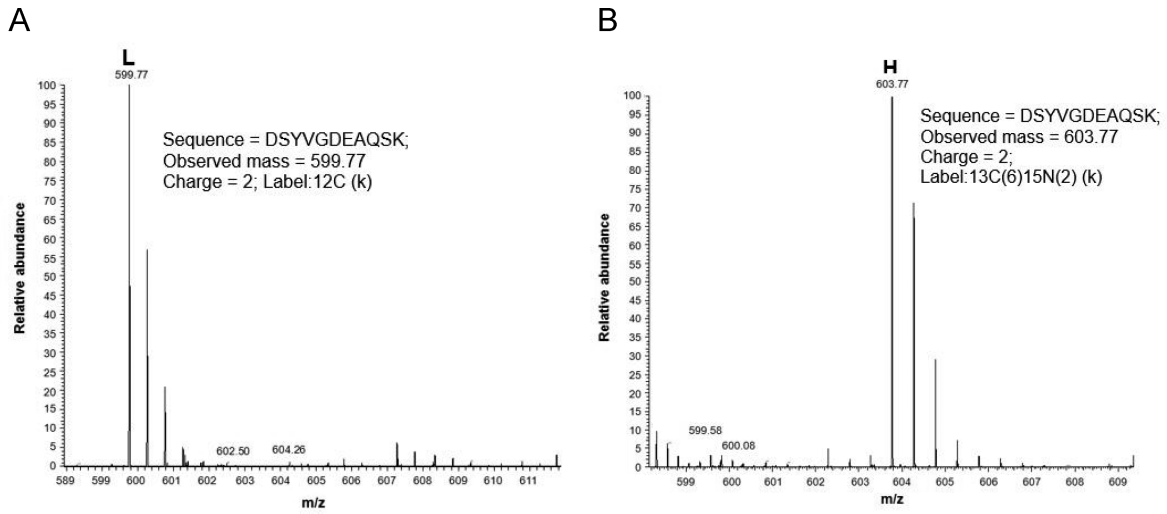

Figure 1. Incorporation efficiency of heavy and light amino acids into the KGN cells by an Orbitrap mass spectrometer. Peak annotated with L (A) and H (B) is peptide DSYVGDEAQSK of actin, cytoplasmic 1 in untreated KGN cells cultured in SILAC media containing light and heavy amino acids, respectively. The observed mass of peptide DSYVGDEAQSK is 599.75 and 603.77 after incorporation of the ^{12}C6-lysine (L) and ^{13}C6-^{15}N2-lysine (H), respectively. Incorporation efficiency is calculated by the ratio of the relative abundance of the light and heavy forms of actin in the "heavy" KGN cells (panel B), which is >99%.

and lysed with 5 mL of cold Farnham lysis buffer (5 mM PIPES pH 8.0, 85 mM KCL, 0.5% Nonidet P-40, Roche cOmplete EDTA-free protease inhibitor cocktail tablet). Cells were pelleted at 2000 rpm for 5 min at 4 °C and then passed through a 21-gauge needle 20 times. Following centrifugation at 2000 rpm for 5 min at 4 °C, the supernatant was removed and the pellet was resuspended in 300 μL of cold RIPA buffer (1× PBS, 1% NP-40, 0.5% sodium deoxycholate, 0.1% SDS, Roche cOmplete EDTA-free protease inhibitor cocktail tablet). The DNA was sheared with a Covaris S220 Focused-ultrasonicator in a circulating water bath using the following parameters: peak power of 105 W, duty factor of 2, and 200 cycles per burst for 4 min at 4 °C. 50 μL of the sonicated DNA was set aside as the input DNA.

Immunoprecipitation

250 μL of chromatin was incubated with 50 μL of goat antirabbit IgG magnetic beads (New England Biolabs, Ipswich, MA) precoupled to 5 μg of anti-PPARγ antibody (Abcam no. ab45036) on a rotator platform for 1 h at 4 °C. Beads containing immune-bound chromatin were washed five times with cold IP wash buffer (100 mM Tris pH 7.5, 500 mM lithium chloride, 1% NP-40, 1% sodium deoxycholate) with mixing for 3 min for each wash on a rotator. Following washing and mixing with 1 mL of TE buffer (10 mM Tris-HCl pH7.5, 0.1 mM Na_2EDTA) for 1 min on the rotator, the bead pellet was resuspended in 200 μL of IP elution buffer (1% SDS, 0.1 M $NaHCO_3$). To elute the immune-bound chromatin from the beads, the bead pellet was incubated in a 65 °C water bath for 1 h and vortexed every 15 min. The supernatant containing the DNA was collected following centrifugation at 14 000 rpm at room temperature for 3 min. The cross-linking was reversed by incubation in a 95 °C water bath for 15 min.

400 μg of proteinase K (Roche Applied Science) was added to the DNA and incubated at room temperature for 2 min. The DNA was then cleaned up using the PCR purification kit (Qiagen, Hilden, Germany) according to the manufacturer's instructions. The DNA was eluted in two 15 μL aliquots of warmed buffer EB.

Confirmation of PPARγ Putative Binding Sites

PCR amplifying the putative binding site was performed to confirm PPARγ binding on *SCD*. Primers were as follows: for −3293 to −3274, sense, 5′-CCACCAATCTACTTTCTG-TCTC-3′ and antisense, 5′-GGTAACAAAGTGAGACCCT-ATC-3′; for −7908 to −7889, sense, 5′-GGCAGCTGTGGC-ATAGTCA-3′ and antisense, 5′-GGGCTGAGGCTGTCA-TTTCT-3′. The samples were denatured at 95 °C for 5 min and amplified for 32 (−3293 to −3274) or 27 (−7908 to −7889) cycles at 95 °C for 30 s, 60 °C for 30 s, and 72 °C for 40 s, with a final extension step at 72 °C for 7 min. The PCR products were loaded on a 1.5% agarose gel stained with SYBR Safe (Thermo Fisher Scientific).

Statistical Analyses

Drug treatments for ChIP, RNA, or protein extraction were performed in duplicate and repeated at least three times. Data are presented as mean ± SD. One-way ANOVA or the nonparametric equivalent Kruskal−Wallis test was used for statistical analyses, where $P < 0.05$ is considered statistically significant.

RESULTS

Combined XIAP inhibition (CmpdA or Emb) and PPARγ (RGZ and RA) activation leads to the induction of apoptosis in human GCT-derived cell lines.[5] To understand the underlying mechanisms of this response, we utilized SILAC to identify the proteomic changes. The incorporation of the heavy and light amino acids was confirmed using mass spectrometry prior to drug treatment in the KGN cells (Figure 1). Altogether, a total of 569 proteins were identified in the KGN cells after CmpdA/RGZ/RA or Emb/RGZ/RA treatment. Of these, 22 were upregulated and 10 were downregulated by ≥1.5 fold after the combined treatment (Tables 1 and 2). We then used the *Search Tool for the Retrieval of Interacting Genes/Proteins* (STRING v10) to identify any interactions between the regulated proteins and classify these proteins according to their biological processes. GO enrichment analysis identified several subsets of proteins that were

DOI: 10.1021/acs.jproteome.8b00917
J. Proteome Res. 2019, 18, 1691−1702

Table 1. Upregulated Proteins in KGN Cells[a]

protein ID	gene	protein	average ratio		peptides identified	protein score	% sequence coverage
			CmpdA/RGZ/RA	Emb/RGZ/RA			
O00767	SCD	stearoyl-CoA desaturase	4.5	4.59	5	87	3.6
						344	10.6
P08648[b]	ITA5	integrin α-5	nd	3.23	3		2.6
						53	4.1
P00558	PGK1	phosphoglycerate kinase I	nd	2.87	18	875	55.6
						1118	53.5
O95573	ACSL3	Acyl-CoA synthetase long chain family member 3	nd	2.56	6	51	4.4
						84	5.6
P07602	PSAP	prosaposin	1.79	2.32	10	CmpdA/RGZ/RA:	CmpdA/RGZ/RA:
						361	22.1
						190	9.4
						Emb/RGZ/RA:	Emb/RGZ/RA:
						177	7.3
						240	19.3
P21980[b]	TGM2	protein-glutamine γ-glutamyltransferase 2	2.3	nd			2.6
						221	9.3
P08670	VIM	vimentin	2.21	nd	40	4165	84.5
						2682	69.5
P07858	CTSB	cathepsin B	1.56	1.97	7	CmpdA/RGZ/RA:	CmpdA/RGZ/RA:
						225	19.2
						254	18
						Emb/RGZ/RA:	Emb/RGZ/RA:
						170	10
						362	23.9
P61769	B2M	beta 2 microglobulin	1.74	1.9	2	CmpdA/RGZ/RA:	CmpdA/RGZ/RA:
						83	26.9
						28	26.9
						Emb/RGZ/RA:	Emb/RGZ/RA:
						79	26.9
						141	26.9
P04083	ANXA1	annexin A1	nd	1.83	20	759	50.9
						43	2.7
P11279[b]	LAMP1	lysosome-associated membrane glycoprotein 1	nd	1.75	3		6.8
						134	14.4
Q16777	H2A2C	histone H2A type 2-C	1.7	nd	5	273	35.9
						95	14
P00338	LDHA	L-lactate dehydrogenase A chain	nd	1.69	21	158	15.7
P13473[b]	LAMP2	lysosome-associated membrane glycoprotein 2	nd	1.67	3		9.7
						1422	72.9
Q13162	PRDX4	peroxiredoxin-4	nd	1.67	6	84	16.6
						290	21
P60174	TPI1	triosephosphate isomerase	nd	1.64	12	693	54.2
						705	52.8
P07237	P4HB	protein disulfide isomerase	nd	1.59	9	149	12.8
						274	15.9
P45880[b]	VDAC2	voltage-dependent anion-selective channel protein 2	1.57	nd			5.7
							9.9
P17516[b]	AKRIC4	aldo-keto reductase family 1 member C4	1.56	nd		133	15.8
						58	8
P06733	ENO1	alpha enolase	nd	1.55	31	1456	68.4
						1790	78.6
P11021	HSPA5	78 kDa glucose-regulated protein	nd	1.52	21	828	29.5
						1299	37
P07339	CTSD	cathepsin D	1.51	nd	17	606	26.9
						1284	46.4

[a]Mass spectrometry analysis identified 22 proteins that were upregulated by ≥1.5 fold by the 24 h combination treatment in the KGN cells. Protein ratios from the reciprocal experiments were averaged to calculate the final fold change. Protein scores and sequence coverage for each individual protein from the reciprocal experiments are listed. nd, not detected. [b]Six proteins were previously identified, but because of a change of personnel

DOI: 10.1021/acs.jproteome.8b00917
J. Proteome Res. 2019, 18, 1691−1702

Table 1. continued

for analysis, these were not found in the final list of differentially expressed proteins. These proteins were excluded from the GO enrichment analysis.

Table 2. Downregulated Proteins in KGN Cells[a]

protein ID	gene	protein	average ratio		peptides identified	protein score	% sequence coverage
			CmpdA/RGZ/RA	Emb/RGZ/RA			
P49411	TUFM	elongation factor Tu, mitochondrial	nd	−2.7	13	14	14
						719	30.5
O94925[b]	GLSK	glutaminase	−1.64	nd	1	234	5.4
						234	5.4
Q16695	HIST3H3	histone H3.1	nd	−1.99	8	289	54.4
						300	54.4
Q07021[b]	C1QBP	complement component 1Q subcomponent-binding protein, mitochondrial	nd	−1.98			14.5
							14.5
P35579	MYH9	myosin-9	nd	−1.81	32	1952	30.1
						3291	36.6
P40926[b]	MDHM	malate dehydrogenase	nd	−1.76			13.4
						54	21.6
P05141	SLC25A5	ADP/ATP translocase 2	nd	−1.57	9	174	29.2
						195	14.8
P62249[b]	RS16	40S ribosomal protein S16	nd	−1.51	1		23
						75	23
P62263[b]	RS14	40S ribosomal protein S14	nd	−1.5			10.8
							10.8
Q16658	FSCN1	fascin	−1.65	nd	4	277	8.5
						188	7.5

[a]10 proteins were found to be downregulated by ≥1.5 fold after the combined treatment in the KGN cells for 24 h. Protein ratios from the reciprocal experiments were averaged to calculate the final fold change. nd, not detected. [b]Five proteins were previously identified, but because of a change of personnel for analysis, these were not found in the final list of differentially expressed proteins. These proteins were excluded from the GO enrichment analysis.

enriched for various steps involved in the canonical glycolysis pathways ($P < 0.05$) (Table 3). The significant upregulation of metabolic pathways is consistent with the restoration of PPARγ activity upon the removal of the NF-κB transrepression by the XIAP inhibitors, CmpdA and Emb. No pathway was found to be over- or under-represented among the down-regulated proteins.

Stearoyl-CoA Desaturase Was Upregulated by Combined XIAP and PPARγ Treatment

Among the 22 upregulated and 10 downregulated proteins, stearoyl-CoA desaturase (SCD) showed the greatest fold change after CmpdA/RGZ/RA treatment compared with vehicle. Orbitrap mass spectrometry analysis identified 4.5- and 4.6-fold (average change of reciprocal experiments) induction in SCD in the KGN cells after combined CmpdA/RGZ/RA and Emb/RGZ/RA treatment, respectively (Figure 2A and Table 1).

In KGN cells, Western blot analysis demonstrated that SCD protein levels were significantly increased after CmpdA/RGZ/RA (3.5-fold) and Emb/RGZ/RA (4.3-fold) treatment (Figure 2B,C), confirming the mass spectrometry findings. We also investigated the response of SCD at the mRNA level. SCD is encoded by the stearoyl-CoA desaturase (*SCD*) gene. Digital PCR using the Fluidigm Biomark HD system demonstrated that *SCD* mRNA was upregulated by 3.3- and 4.0-fold after 24 h of treatment with CmpdA/RGZ/RA and Emb/RGZ/RA in the KGN cells, respectively (Figure 2D).

Upregulation of Proteins and Genes Associated with Metabolism

Besides SCD, the functional annotation of differentially regulated proteins performed by GO enrichment analysis revealed an over-representation of the canonical glycolysis pathway ($P < 0.05$) (Table 3). Following selection based on the magnitude of change, we quantified the mRNA levels of the mRNA that encodes for the proteins involved in this biological process using the Fluidigm Biomark HD system. In addition to SCD, we also identified other targets that are regulated by the combined PPARγ and XIAP treatment. These include acyl-CoA synthetase long-chain family member 3 (ACSL3) and α-enolase (ENO1). ACSL3 protein levels were significantly increased by Emb/RGZ/RA (Table 1), and *ACSL3* gene expression was increased by both CmpdA/RGZ/RA and Emb/RGZ/RA treatment (Figure 3A). Similarly, ENO1 demonstrated a consistent induction at both the mRNA (Figure 3B) and protein (Table 1) levels following Emb/RGZ/RA treatment.

PPARγ Binding Sites on SCD Promoter Region

SCD plays a role in fatty acid and cholesterol synthesis.[38] To date, no known function of SCD in the granulosa cells of the ovary has been documented. It has previously been shown that PPARγ agonists increase SCD protein and mRNA in adipose tissue.[38,39] However, there are no reports that describe PPARγ binding sites in the promoter. Our screening identified two putative binding sites for PPARγ between nucleotides points

DOI: 10.1021/acs.jproteome.8b00917
J. Proteome Res. 2019, 18, 1691−1702

Table 3. GO Enrichment Analysis[a]

GO biological process	Homo sapiens REF #	#	Expected value	Fold enrichment	*P* value
Canonical glycolysis	27	3	0.02	>100	0.01
- Glucose catabolic process to pyruvate	27	3	0.02	>100	0.01
- Pyruvate metabolic process	69	4	0.05	75.99	0.00175
- Monocarboxylic acid metabolic process	481	6	0.37	16.35	0.00812
- Carboxylic acid metabolic process	868	8	0.66	12.08	0.000698
- Oxoacid metabolic process	976	8	0.74	10.74	0.00172
- Organic acid metabolic process	993	8	0.76	10.56	0.00196
- Single-organism cellular process	9841	16	7.51	2.13	0.0469
- Single-organism metabolic process	3572	12	2.73	4.40	0.00465
	30	3	0.02	>100	0.0137
- Glucose catabolic process	108	4	0.08	48.55	0.0103
- Single-organism carbohydrate catabolic process	115	4	0.09	45.59	0.0133
	847	7	0.65	10.83	0.0123
- Carbohydrate catabolic process	27	3	0.02	>100	0.01
- Single-organism catabolic process	951	7	0.73	9.65	0.0266
- NADH regeneration	36	3	0.03	>100	0.0237
- Oxidation-reduction process	70	4	0.05	74.90	0.00186
- NADH metabolic process	112	4	0.09	46.81	0.0119
- NAD metabolic process	112	4	0.09	46.81	0.0119
- Nicotinamide nucleotide metabolic process	118	4	0.09	44.43	0.0147
- Pyridine nucleotide metabolic process	128	4	0.10	40.96	0.0202
- Pyridine-containing compound metabolic process	289	6	0.22	27.21	0.000414
	360	6	0.27	21.85	0.0015
- Oxidoreduction coenzyme metabolic process	28	3	0.02	>100	0.0112
	28	3	0.02	>100	0.0112
- Coenzyme metabolic process	40	4	0.03	>100	0.000201
- Cofactor metabolic process	41	4	0.03	>100	0.000222
- Glycolytic process through glucose-6-phosphate	47	4	0.04	>100	0.000382
- Glycolytic process through fructose-6-phosphate	63	4	0.05	83.22	0.00122
- Glycolytic process	63	4	0.05	83.22	0.00122
- ATP generation from ADP	84	4	0.06	62.42	0.00383
- ADP metabolic process	65	4	0.05	80.66	0.00138
- Purine ribonucleoside diphosphate metabolic process	58	4	0.04	90.40	0.00088
	64	4	0.05	81.92	0.0013
- Purine nucleoside diphosphate metabolic process					
- Nucleoside diphosphate metabolic process					
- Ribonucleoside diphosphate metabolic process					
- Nucleoside diphosphate phosphorylation					
- Nucleoside phosphorylation					
Gluconeogenesis	45	3	0.03	87.38	0.046

[a]GO enrichment analysis was performed on the genes that encode the 16 upregulated proteins identified from the SILAC study. GO biological processes that are over-represented for this set of genes are listed. *Homo sapiens* REF # indicates the number of genes in the selected organism (i.e., *Homo sapiens*) that share the same GO biological process category; total number of genes in the *Homo sapiens* REF list is 20 972. # refers to number of genes in our data set that are mapped to a particular category. Expected value refers to the number of genes one would expect in an analyzed data set for a certain GO biological process. In the case of an over-representation, more genes (#) from the analyzed data set are identified for a biological process than expected ("Expected value"). Fold enrichment of >1 means that the biological process is overrepresented in the data set. *P* value is the probability of the number of identified genes being annotated in the category by chance.

−7908 to −7889 and −3293 to −3274 relative to the start site of transcription.

Following 6 h of drug treatment with DMSO, RGZ/RA, or CmpdA/RGZ/RA, ChIP-PCR analysis demonstrated a significant increase in PPARγ binding at the region −3293 to −3274 (Figure 4). There appears to be a small increase at −7908 to −7889; however, this is not significant (Figure 4).

Detection of SCD, ACSL3, and ENO1 in Untreated KGN Cells and Human GCT Samples

We have previously performed a whole transcriptome analysis of 12 human GCT and the KGN cells,[40] which enabled us to analyze the levels of *SCD*, *ACSL3*, and *ENO1* mRNA in untreated KGN cells and human GCT using this data set. *SCD* mRNA was detected in all samples. The levels do not differ by stage. The stage (stage 1 versus recurrent) of the disease does not alter the level of expression; the KGN cells showed a similar level of *SCD* mRNA as the human GCT samples (Figure 5). Similarly, ACSL3 and ENO1 were both detected in all samples with similar levels of expression in the stage-1 and recurrent GCT (Supplementary Figure 1). Statistical analysis was not performed with only one cell line from three replicate experiments included in the data set.

DISCUSSION

XIAP is considered as an attractive therapeutic target due to its impact on both the intrinsic and extrinsic apoptotic pathways.[18] XIAP inhibitors, SMAC-mimetics, which mimic the function of endogenous SMAC, have been tested as antitumor agents in clinical trials.[28,29,41] Downregulation of XIAP has also

DOI: 10.1021/acs.jproteome.8b00917
J. Proteome Res. 2019, 18, 1691−1702

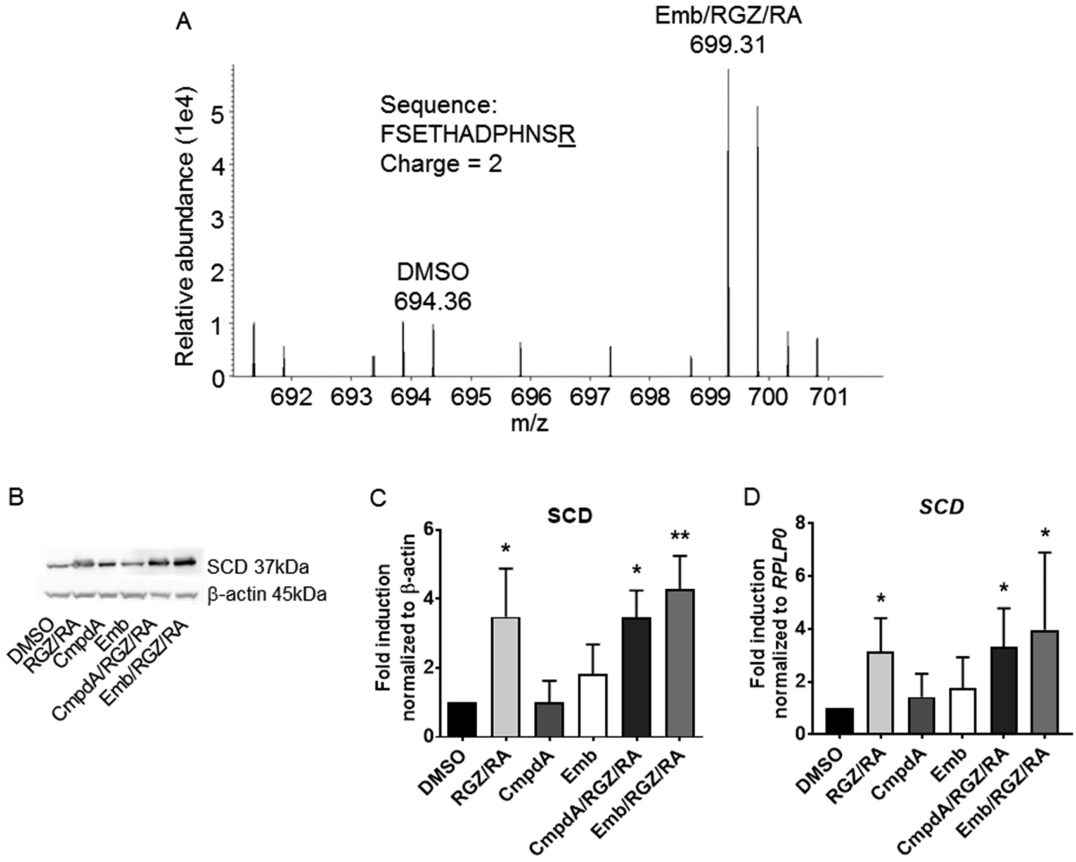

Figure 2. SCD protein and mRNA levels in KGN cells. (A) Spectrum of one of the unique SCD peptide sequences showing the upregulation of SCD following Emb/RGZ/RA treatment. Emb/RGZ/RA-treated KGN cells were labeled with ^{13}C6-^{15}N4-arginine (*Arg-10*), whereas DMSO control was labeled with ^{12}C6-arginine. (B) Western blot of SCD with β-actin as loading control. (C) Densitometry analysis of Western blot of SCD expression (normalized to β-actin) following 24 h of treatment of RGZ/RA, CmpdA/RGZ/RA, or Emb/RGZ/RA in KGN. n = 3; mean ± SD; one-way ANOVA; Bonferroni posthoc analysis. *P < 0.01; **P < 0.005 when compared with DMSO. (D) *SCD* mRNA expression (normalized to *RPLP0*) following 24 h of treatment of RGZ/RA, CmpdA/RGZ/RA, or Emb/RGZ/RA in KGN demonstrated using digital PCR. n = 4−7; mean ± SD; Kruskal−Wallis test; Dunn's posthoc analysis. *P < 0.05 when compared with DMSO.

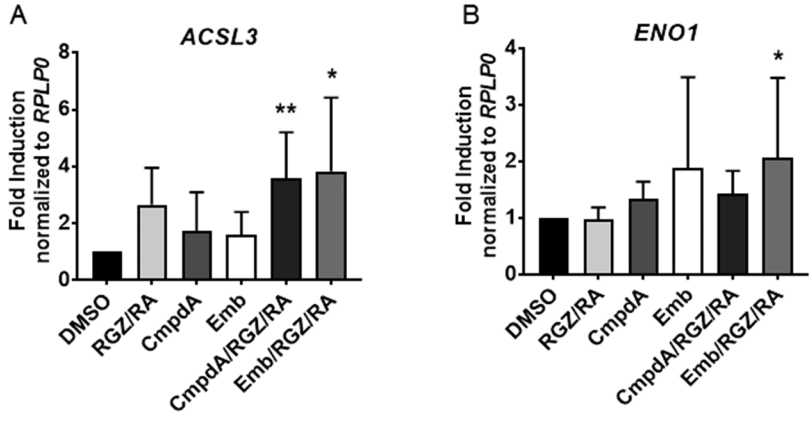

Figure 3. *ACSL3* and *ENO1* mRNA level in KGN cells. *ACSL3* (A) and *ENO1* (B) mRNA expression following drug treatments in KGN using digital PCR. mRNA expression was normalized to that of RPLP0. n = 4−7; mean ± SD; Kruskal−Wallis test; Dunn's posthoc analysis. *P < 0.05; **P < 0.01 when compared with DMSO.

been shown to induce apoptosis in chemoresistant human ovarian cancer cell lines.[42,43] Although originally designed to inactivate XIAP, SMAC-mimetics such as Compound A are also effective in producing rapid ubiquitylation and proteosomal degradation of cIAP1,[44,45] another member of the IAP family, which also binds to caspases-3, -7, and -9 but with a lower affinity than XIAP.[46] We have shown that XIAP is the predominant IAP expressed in GCT, and the levels of other members are low.[5] Thus the effect that we see is likely XIAP-specific.

PPARγ is a transcription factor that promotes differentiation and induces apoptosis in the ovary.[10] PPARγ is also involved in the regulation of lipid and glucose metabolism. The modulation of PPARγ action using TZD has also been found

DOI: 10.1021/acs.jproteome.8b00917
J. Proteome Res. 2019, 18, 1691−1702

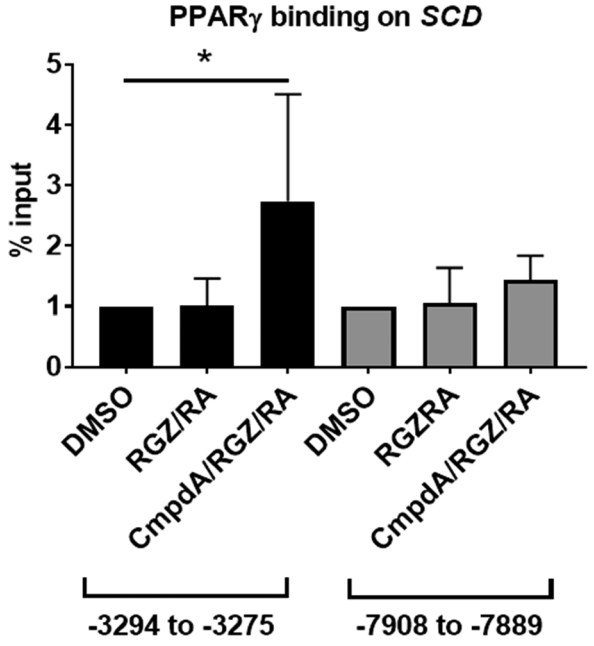

Figure 4. ChIP-PCR analysis of PPARγ binding on *SCD* promoter region in KGN. PPARγ binding on *SCD* at nucleotide points −3294 to −3275 and −7908 to −7889 was investigated in the KGN cells following treatment with DMSO (control), RGZ/RA, or CmpdA/RGZ/RA for 6 h. Binding intensity following singular treatment, RGZ/RA, was not significant. $n = 4$; mean ± SD; Kruskal−Wallis test; Dunn's posthoc analysis; $^*P < 0.05$ when compared with DMSO.

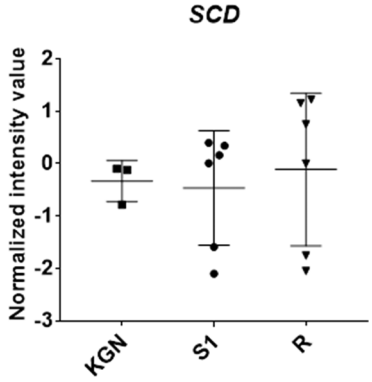

Figure 5. Microarray analysis of *SCD* mRNA in the KGN cells, stage-1, and recurrent GCT. Values were averaged and normalized over three replicate samples of the KGN cell line and six stage-1 (S1) and six recurrent (R) GCT samples.

to exert antineoplastic effects in various solid tumors.[14−16] The pro-differentiative role of PPARγ has been shown to inhibit tumor development and progression.[12] Previous studies have demonstrated the overexpression of PPARγ in many tumor types and in various cancers, such as those that arise from the colon[13] and thyroid,[47] where activation of PPARγ reduced the cell viability and inhibited cell proliferation. These antitumor effects of PPARγ agonists have also been observed in the xenograft model of solid tumors.[48]

As might be anticipated, the use of XIAP inhibitors or PPARγ agonists as anticancer treatment has been shown to be more efficient in malignancies that express the XIAP or PPARγ proteins.[12,22] As with GCT, several cancers have been reported to coexpress XIAP and PPARγ proteins including glioblastoma,[49] colon cancer,[50,51] and leukemia.[52] In these studies, XIAP inhibition using a SMAC-mimetic, Compound A,[52] or XIAP knockdown[51] sensitized the cancers to PPARγ-dependent cell death induced by TZD in vitro and in vivo, whereas monotherapy targeting XIAP or PPARγ alone did not affect apoptosis or proliferation. Moreover, PPARγ antagonist, GW9662, rescued cells from apoptosis in vitro, indicating PPARγ dependence in the anticancer effects.[52]

We have found that combining an XIAP inhibitor with PPARγ agonists induces both differentiation and apoptosis in GCT cells.[5] In the current study, we have sought to understand the mechanism of the response using SILAC labeling coupled to mass spectrometry analysis to investigate the proteomic changes in the cells following the combined treatment.

Of the 32 proteins that were differentially regulated by the combined treatment, SCD stands out as the most interesting target with the greatest magnitude of change. SCD mRNA and protein levels are upregulated by both CmpdA/RGZ/RA and Emb/RGZ/RA treatment in the KGN cells. Furthermore, we provide evidence that this is a transcriptional response mediated via a direct interaction of PPARγ with the *SCD* gene.

Stearoyl-CoA desaturase (SCD), also called Δ-9-desaturase, converts saturated fatty acids to monounsaturated fatty acids (MUFAs), namely, palmitoyl- and stearoyl-CoA to palmitoleic and oleic acid, which are preferred substrates for cholesterol biosynthesis. SCD is predominantly expressed by adipocytes but is also detected in other organs including the ovary. We have examined the levels of SCD in six stage-1, six recurrent GCT, and KGN cells using microarray analysis.[40] *SCD* mRNA was detected in all samples; no significant difference was observed among the GCT samples, regardless of the stage of disease, and the untreated KGN cells.

There is no existing literature on the function of SCD in the ovary. Arguably, it may have a role in steroidogenesis given its function in synthesizing cholesterol, the precursor for steroidogenesis. Zhao and colleagues[53] identified in a group of women with polycystic ovarian syndrome (PCOS) an increase in the MUFA to saturated fatty acids ratio, which is indicative of increased SCD activity. No direct link has been reported between PCOS and SCD, but it is plausible that the hormone imbalance and increased cholesterol level are associated with the heightened SCD activity in PCOS patients.[53]

Altered SCD expression has been associated with the metabolic syndrome.[54] Previous studies have consistently reported that SCD expression is increased upon PPARγ activation by TZD in individuals with diabetes. Treatment with the antidiabetic TZD, including one that was used in this study, RGZ,[39] as well as pioglitazone[38] increased *SCD* mRNA and protein expression in adipose tissues and adipocytes of humans with varying insulin sensitivity. These subjects demonstrated improved insulin sensitivity after TZD treatment. However, it is difficult to determine from these studies if it is a primary or secondary effect of PPARγ activation given that the treatments varied between hours and days in vitro and months in vivo. Despite the activation, no existing literature has reported direct evidence that PPARγ regulates/activates SCD expression or activity. Using promoter analysis, we identified two putative binding sites of PPARγ to the promoter region of *SCD*; cells treated with XIAP inhibitor and PPARγ agonist showed an increase in *SCD* gene expression.

ACSL3 catalyzes long-chain fatty acids to form acyl-CoA in fatty acid metabolism. It is expressed in various tissues, including the ovary. No specific role of ACSL3 in the ovary has

DOI: 10.1021/acs.jproteome.8b00917
J. Proteome Res. 2019, 18, 1691−1702

been described. Bu and colleagues[55] reported that ACSL3 siRNA suppressed PPARγ transcriptional activity in hepatocytes, suggesting a positive relationship between ACSL3 and PPARγ. In our study, we found that ACSL3 mRNA and protein expression was upregulated following the restoration of PPARγ activity. This points to a possible reciprocity in the regulation. A downregulation of ACSL3 was noted in 1648 ovarian cancers, and higher expression was correlated with a better prognosis in these patients.[56] From the microarray analysis of six stage-1, six recurrent GCT, and the KGN cells,[40] the levels of ACSL3 were similar regardless of the stage of the disease; no difference was observed compared with the untreated KGN cells (Supplementary Figure 1A).

The glycolytic enzyme, α-enolase (ENO1), catalyzes the production of phosphoenolpyruvate from 2-phospho-D-gylcerate in the cytoplasm.[57] A short variant of ENO1, Myc promoter-binding protein-1 (MBP-1), represses Myc transcription in the nucleus and may serve as a tumor suppressor.[57] ENO1 is widely expressed across the body. *ENO1* mRNA expression was observed in GC and theca cells of the rat ovary,[58] and ENO1 protein was detected in the human ovary.[59] *ENO1* mRNA expression remained unchanged throughout the estrous cycle and was not altered by human chorionic gonadotropin (hCG).[60] No difference in *ENO1* mRNA expression was observed between KGN cells, stage-1, or recurrent GCT (Supplementary Figure 1B). Consistent with potential tumor suppressive effects, knockdown of ENO1 using siRNA has been shown to increase cell growth in Chinese hamster ovary (CHO) cells.[61]

The increased expression of targets associated with metabolism is consistent with the restoration of PPARγ activity. This is achieved by the release of PPARγ from transrepression by NF-κB through the inhibition of XIAP. Despite the link of heightened metabolism with unfavorable outcomes in cancer, we found using extracellular flux analysis that the GCT-derived cells subjected to the combined treatment are less metabolically active.[5] Additionally, these cells failed to respond to the increased energy demand under stressed conditions. The combined XIAP and PPARγ approach also induced apoptosis in the GCT-derived cells, as shown by high content screening.[5]

CONCLUSIONS

This proteomic analysis is a proof of concept that the transrepression of PPARγ signaling can be removed by a small molecular inhibitor of XIAP in the GCT cells. Without the repressive effect, the antineoplastic function of PPARγ is reinstated by PPARγ agonists. Coexpression of XIAP and PPARγ at high levels is seen not only in the GCT but also in other solid tumors. This phenomenon thus makes these two proteins unique candidates for a targeted therapy that has a broader implication beyond GCT.

ASSOCIATED CONTENT

Supporting Information

The Supporting Information is available free of charge on the ACS Publications website at DOI: 10.1021/acs.jproteome.8b00917.

Supplementary Figure 1. Microarray analysis of *ACSL3* and *ENO1* mRNA in the KGN cells, stage-1, and recurrent GCT (PDF)

AUTHOR INFORMATION

Corresponding Author

*Tel: +61385722545. Fax: +61395946125. E-mail: simon.chu@hudson.org.au.

ORCID

Dilys T. H. Leung: 0000-0002-3504-2134

Adam Rainczuk: 0000-0002-0813-1107

Present Address

§D.T.H.L.: Fiona Elsey Cancer Research Institute, 106−110 Lydiard Street South, Ballarat Central, Victoria 3350, Australia.

Author Contributions

The manuscript was written through contributions of all authors. All authors have given approval to the final version of the manuscript.

Notes

The authors declare no competing financial interest.

The mass spectrometry proteomics data have been deposited to the ProteomeXchange Consortium via the PRIDE[34] partner repository with the data set identifier PXD012509.

ACKNOWLEDGMENTS

We acknowledge Dr. Peter Hoffmann and Dr. Georgia Arentz at Adelaide Proteomics Centre for mass spectrometry analysis of the samples, Maria Alexiadis for the microarray data, and the MHTP Medical Genomics Facility, Melbourne, Australia as the service provider for quantitative PCR. This work was supported by grants-in-aid from the Cancer Council Victoria; the Ovarian Cancer Research Foundation and the Rivkin Centre (SC); the Granulosa Cell Tumor of the Ovary Foundation; the National Health & Medical Research Council of Australia through a project grant (grant number 1058334); the DoD CDMRP, grant number W81XWH-17-OCRP-IIRA-cfda12.420; and an Endocrine Society of Australia Research Higher Degree Scholarship to D.T.H.L. We would like to acknowledge the MHTP medical Genomics Facility, Melbourne, Australia, as the service provider for quantitative Digital PCR Fluidigm Analysis. The Hudson Institute and the Walter and Eliza Hall Institute are supported by the Victorian Government's Operational Infrastructure Scheme.

ABBREVIATIONS

ACSL3, acyl-CoA synthetase long-chain family member 3; CmpdA, Compound A; Emb, embelin; ENO1, α-enolase; GCT, granulosa cell tumors; PPARγ, peroxisome proliferator-activated receptor gamma; RA, retinoic acid; RGZ, rosiglitazone; SCD, stearoyl-CoA desaturase; TZD, thiazolidinedone; XIAP, X-linked inhibitor of apoptosis protein

REFERENCES

(1) Jamieson, S.; Fuller, P. J. Molecular pathogenesis of granulosa cell tumors of the ovary. *Endocr. Rev.* **2012**, *33* (1), 109−44.

(2) Fuller, P. J.; Leung, D.; Chu, S. Genetics and genomics of ovarian sex cord-stromal tumors. *Clin. Genet.* **2017**, *91* (2), 285−291.

(3) Nishi, Y.; Yanase, T.; Mu, Y.; Oba, K.; Ichino, I.; Saito, M.; Nomura, M.; Mukasa, C.; Okabe, T.; Goto, K.; Takayanagi, R.; Kashimura, Y.; Haji, M.; Nawata, H. Establishment and characterization of a steroidogenic human granulosa-like tumor cell line, KGN, that expresses functional follicle-stimulating hormone receptor. *Endocrinology* **2001**, *142* (1), 437−45.

(4) Jamieson, S.; Butzow, R.; Andersson, N.; Alexiadis, M.; Unkila-Kallio, L.; Heikinheimo, M.; Fuller, P. J.; Anttonen, M. The FOXL2

DOI: 10.1021/acs.jproteome.8b00917
J. Proteome Res. 2019, 18, 1691−1702

C134W mutation is characteristic of adult granulosa cell tumors of the ovary. *Mod. Pathol.* **2010**, *23* (11), 1477−85.
(5) Leung, D. T. H.; Nguyen, T.; Oliver, E. M.; Matti, J.; Alexiadis, M.; Silke, J.; Jobling, T. W.; Fuller, P. J.; Chu, S. Combined PPARg activation and XIAP inhibition as a potential therapeutic strategy for ovarian granulosa cell tumors. *Mol. Cancer Ther.* **2019**, *18*, 364.
(6) Alexiadis, M.; Eriksson, N.; Jamieson, S.; Davis, M.; Drummond, A. E.; Chu, S.; Clyne, C. D.; Muscat, G. E.; Fuller, P. J. Nuclear receptor profiling of ovarian granulosa cell tumors. *Horm. Cancer* **2011**, *2* (3), 157−69.
(7) Chu, S.; Alexiadis, M.; Fuller, P. J. Proteasome inhibition by bortezomib decreases proliferation and increases apoptosis in ovarian granulosa cell tumors. *Reprod. Sci.* **2009**, *16* (4), 397−407.
(8) Aleman-Gonzalez-Duhart, D.; Tamay-Cach, F.; Alvarez-Almazan, S.; Mendieta-Wejebe, J. E. Current Advances in the Biochemical and Physiological Aspects of the Treatment of Type 2 Diabetes Mellitus with Thiazolidinediones. *PPAR Res.* **2016**, *2016*, 7614270.
(9) Long, M. J.; Sairam, M. R.; Komar, C. M. Initiation of the expression of peroxisome proliferator-activated receptor gamma (PPAR gamma) in the rat ovary and the role of FSH. *Reprod. Biol. Endocrinol.* **2009**, *7*, 145.
(10) Froment, P.; Gizard, F.; Defever, D.; Staels, B.; Dupont, J.; Monget, P. Peroxisome proliferator-activated receptors in reproductive tissues: from gametogenesis to parturition. *J. Endocrinol.* **2006**, *189* (2), 199−209.
(11) Zhang, H.; Li, Q.; Lin, H.; Yang, Q.; Wang, H.; Zhu, C. Role of PPARgamma and its gonadotrophic regulation in rat ovarian granulosa cells in vitro. *Neuro Endocrinol Lett.* **2007**, *28* (3), 289−94.
(12) Ferrari, S. M.; Materazzi, G.; Baldini, E.; Ulisse, S.; Miccoli, P.; Antonelli, A.; Fallahi, P. Antineoplastic Effects of PPARgamma Agonists, with a Special Focus on Thyroid Cancer. *Curr. Med. Chem.* **2016**, *23* (7), 636−49.
(13) Tsukahara, T.; Haniu, H. Peroxisome proliferator-activated receptor gamma overexpression suppresses proliferation of human colon cancer cells. *Biochem. Biophys. Res. Commun.* **2012**, *424* (3), 524−9.
(14) Komatsu, Y.; Yoshino, T.; Yamazaki, K.; Yuki, S.; Machida, N.; Sasaki, T.; Hyodo, I.; Yachi, Y.; Onuma, H.; Ohtsu, A. Phase 1 study of efatutazone, a novel oral peroxisome proliferator-activated receptor gamma agonist, in combination with FOLFIRI as second-line therapy in patients with metastatic colorectal cancer. *Invest. New Drugs* **2014**, *32* (3), 473−80.
(15) Smallridge, R. C.; Copland, J. A.; Brose, M. S.; Wadsworth, J. T.; Houvras, Y.; Menefee, M. E.; Bible, K. C.; Shah, M. H.; Gramza, A. W.; Klopper, J. P.; Marlow, L. A.; Heckman, M. G.; Von Roemeling, R. Efatutazone, an oral PPAR-gamma agonist, in combination with paclitaxel in anaplastic thyroid cancer: results of a multicenter phase 1 trial. *J. Clin. Endocrinol. Metab.* **2013**, *98* (6), 2392−400.
(16) Murakami, H.; Ono, A.; Takahashi, T.; Onozawa, Y.; Tsushima, T.; Yamazaki, K.; Jikoh, T.; Boku, N.; Yamamoto, N. Phase I study of Efatutazone, an oral PPARgamma agonist, in patients with metastatic solid tumors. *Anticancer Res.* **2014**, *34* (9), 5133−41.
(17) Chu, S.; Nishi, Y.; Yanase, T.; Nawata, H.; Fuller, P. J. Transrepression of estrogen receptor beta signaling by nuclear factor-kappab in ovarian granulosa cells. *Mol. Endocrinol.* **2004**, *18* (8), 1919−28.
(18) Obexer, P.; Ausserlechner, M. J. X-linked inhibitor of apoptosis protein - a critical death resistance regulator and therapeutic target for personalized cancer therapy. *Front. Oncol.* **2014**, *4*, 197.
(19) Phillipps, H. R.; Kokay, I. C.; Grattan, D. R.; Hurst, P. R. X-linked inhibitor of apoptosis protein and active caspase-3 expression patterns in antral follicles in the sheep ovary. *Reproduction* **2011**, *142* (6), 855−67.
(20) Wang, Y.; Rippstein, P. U.; Tsang, B. K. Role and gonadotrophic regulation of X-linked inhibitor of apoptosis protein expression during rat ovarian follicular development in vitro. *Biol. Reprod.* **2003**, *68* (2), 610−9.
(21) Li, J.; Kim, J. M.; Liston, P.; Li, M.; Miyazaki, T.; Mackenzie, A. E.; Korneluk, R. G.; Tsang, B. K. Expression of inhibitor of apoptosis proteins (IAPs) in rat granulosa cells during ovarian follicular development and atresia. *Endocrinology* **1998**, *139* (3), 1321−8.
(22) Li, X.; Chen, W.; Zeng, W.; Wan, C.; Duan, S.; Jiang, S. microRNA-137 promotes apoptosis in ovarian cancer cells via the regulation of XIAP. *Br. J. Cancer* **2017**, *116* (1), 66−76.
(23) Moon, J. H.; Shin, J. S.; Hong, S. W.; Jung, S. A.; Hwang, I. Y.; Kim, J. H.; Choi, E. K.; Ha, S. H.; Kim, J. S.; Kim, K. M.; Hong, D. W.; Kim, D.; Kim, Y. S.; Kim, J. E.; Kim, K. P.; Hong, Y. S.; Choi, E. K.; Lee, J. S.; Hattersley, M.; Jin, D. H.; Kim, T. W. A novel small-molecule IAP antagonist, AZD5582, draws Mcl-1 down-regulation for induction of apoptosis through targeting of cIAP1 and XIAP in human pancreatic cancer. *Oncotarget* **2015**, *6* (29), 26895−908.
(24) Yang, S.; Li, S. S.; Yang, X. M.; Yin, D. H.; Wang, L. Embelin prevents LMP1-induced TRAIL resistance via inhibition of XIAP in nasopharyngeal carcinoma cells. *Oncol. Lett.* **2016**, *11* (6), 4167−4176.
(25) Yang, T.; Lan, J.; Huang, Q.; Chen, X.; Sun, X.; Liu, X.; Yang, P.; Jin, T.; Wang, S.; Mou, X. Embelin sensitizes acute myeloid leukemia cells to TRAIL through XIAP inhibition and NF-kappaB inactivation. *Cell Biochem. Biophys.* **2015**, *71* (1), 291−7.
(26) Holcik, M.; Gibson, H.; Korneluk, R. G. XIAP: apoptotic brake and promising therapeutic target. *Apoptosis* **2001**, *6* (4), 253−61.
(27) Schimmer, A. D.; Dalili, S.; Batey, R. A.; Riedl, S. J. Targeting XIAP for the treatment of malignancy. *Cell Death Differ.* **2006**, *13* (2), 179−88.
(28) Mahadevan, D.; Chalasani, P.; Rensvold, D.; Kurtin, S.; Pretzinger, C.; Jolivet, J.; Ramanathan, R. K.; Von Hoff, D. D.; Weiss, G. J. Phase I trial of AEG35156 an antisense oligonucleotide to XIAP plus gemcitabine in patients with metastatic pancreatic ductal adenocarcinoma. *Am. J. Clin. Oncol.* **2013**, *36* (3), 239−43.
(29) Carter, B. Z.; Mak, D. H.; Morris, S. J.; Borthakur, G.; Estey, E.; Byrd, A. L.; Konopleva, M.; Kantarjian, H.; Andreeff, M. XIAP antisense oligonucleotide (AEG35156) achieves target knockdown and induces apoptosis preferentially in CD34 + 38- cells in a phase 1/2 study of patients with relapsed/refractory AML. *Apoptosis* **2011**, *16* (1), 67−74.
(30) Dean, E. J.; Ranson, M.; Blackhall, F.; Dive, C. X-linked inhibitor of apoptosis protein as a therapeutic target. *Expert Opin. Ther. Targets* **2007**, *11* (11), 1459−71.
(31) Phillipps, H. R.; Hurst, P. R. XIAP: a potential determinant of ovarian follicular fate. *Reproduction* **2012**, *144* (2), 165−76.
(32) Vince, J. E.; Wong, W. W.; Khan, N.; Feltham, R.; Chau, D.; Ahmed, A. U.; Benetatos, C. A.; Chunduru, S. K.; Condon, S. M.; McKinlay, M.; Brink, R.; Leverkus, M.; Tergaonkar, V.; Schneider, P.; Callus, B. A.; Koentgen, F.; Vaux, D. L.; Silke, J. IAP antagonists target cIAP1 to induce TNFalpha-dependent apoptosis. *Cell* **2007**, *131* (4), 682−93.
(33) Nikolovska-Coleska, Z.; Xu, L.; Hu, Z.; Tomita, Y.; Li, P.; Roller, P. P.; Wang, R.; Fang, X.; Guo, R.; Zhang, M.; Lippman, M. E.; Yang, D.; Wang, S. Discovery of embelin as a cell-permeable, small-molecular weight inhibitor of XIAP through structure-based computational screening of a traditional herbal medicine three-dimensional structure database. *J. Med. Chem.* **2004**, *47* (10), 2430−40.
(34) Perez-Riverol, Y.; Csordas, A.; Bai, J.; Bernal-Llinares, M.; Hewapathirana, S.; Kundu, D. J.; Inuganti, A.; Griss, J.; Mayer, G.; Eisenacher, M.; Perez, E.; Uszkoreit, J.; Pfeuffer, J.; Sachsenberg, T.; Yilmaz, S.; Tiwary, S.; Cox, J.; Audain, E.; Walzer, M.; Jarnuczak, A. F.; Ternent, T.; Brazma, A.; Vizcaino, J. A. The PRIDE database and related tools and resources in 2019: improving support for quantification data. *Nucleic Acids Res.* **2019**, *47* (D1), D442−D450.
(35) Szklarczyk, D.; Franceschini, A.; Wyder, S.; Forslund, K.; Heller, D.; Huerta-Cepas, J.; Simonovic, M.; Roth, A.; Santos, A.; Tsafou, K. P.; Kuhn, M.; Bork, P.; Jensen, L. J.; von Mering, C. STRING v10: protein-protein interaction networks, integrated over the tree of life. *Nucleic Acids Res.* **2015**, *43* (D1), D447−52.
(36) The Gene Ontology Consortium. Gene Ontology Consortium: going forward. *Nucleic Acids Res.* **2015**, *43* (D1), D1049−56.

DOI: 10.1021/acs.jproteome.8b00917
J. Proteome Res. 2019, 18, 1691−1702

(37) Mathelier, A.; Fornes, O.; Arenillas, D. J.; Chen, C. Y.; Denay, G.; Lee, J.; Shi, W.; Shyr, C.; Tan, G.; Worsley-Hunt, R.; Zhang, A. W.; Parcy, F.; Lenhard, B.; Sandelin, A.; Wasserman, W. W. JASPAR 2016: a major expansion and update of the open-access database of transcription factor binding profiles. *Nucleic Acids Res.* **2016**, *44* (D1), D110−5.
(38) Yao-Borengasser, A.; Rassouli, N.; Varma, V.; Bodles, A. M.; Rasouli, N.; Unal, R.; Phanavanh, B.; Ranganathan, G.; McGehee, R. E., Jr.; Kern, P. A. Stearoyl-coenzyme A desaturase 1 gene expression increases after pioglitazone treatment and is associated with peroxisomal proliferator-activated receptor-gamma responsiveness. *J. Clin. Endocrinol. Metab.* **2008**, *93* (11), 4431−9.
(39) Kolak, M.; Yki-Jarvinen, H.; Kannisto, K.; Tiikkainen, M.; Hamsten, A.; Eriksson, P.; Fisher, R. M. Effects of chronic rosiglitazone therapy on gene expression in human adipose tissue in vivo in patients with type 2 diabetes. *J. Clin. Endocrinol. Metab.* **2007**, *92* (2), 720−4.
(40) Alexiadis, M.; Chu, S.; Leung, D.; Gould, J. A.; Jobling, T.; Fuller, P. J. Transcriptomic analysis of stage 1 versus advanced adult granulosa cell tumors. *Oncotarget* **2016**, *7* (12), 14207−19.
(41) Fulda, S. Smac Mimetics to Therapeutically Target IAP Proteins in Cancer. *Int. Rev. Cell Mol. Biol.* **2017**, *330*, 157−169.
(42) Ma, J. J.; Chen, B. L.; Xin, X. Y. XIAP gene downregulation by small interfering RNA inhibits proliferation, induces apoptosis, and reverses the cisplatin resistance of ovarian carcinoma. *Eur. J. Obstet. Gynecol. Reprod. Biol.* **2009**, *146* (2), 222−6.
(43) Sasaki, H. S. Y.; Kotsuji, F.; Tsang, B. K. Down-regulation of X-linked inhibitor of apoptosis protein induces apoptosis in chemo-resistant human ovarian cancer cells. *Cancer Res.* **2000**, *60*, 9.
(44) Darding, M.; Feltham, R.; Tenev, T.; Bianchi, K.; Benetatos, C.; Silke, J.; Meier, P. Molecular determinants of Smac mimetic induced degradation of cIAP1 and cIAP2. *Cell Death Differ.* **2011**, *18* (8), 1376−86.
(45) Feltham, R.; Bettjeman, B.; Budhidarmo, R.; Mace, P. D.; Shirley, S.; Condon, S. M.; Chunduru, S. K.; McKinlay, M. A.; Vaux, D. L.; Silke, J.; Day, C. L. Smac mimetics activate the E3 ligase activity of cIAP1 protein by promoting RING domain dimerization. *J. Biol. Chem.* **2011**, *286* (19), 17015−28.
(46) Wei, Y.; Fan, T.; Yu, M. Inhibitor of apoptosis proteins and apoptosis. *Acta Biochim. Biophys. Sin.* **2008**, *40* (4), 278−88.
(47) Antonelli, A.; Ferrari, S. M.; Fallahi, P.; Piaggi, S.; Di Domenicantonio, A.; Galleri, D.; Santarpia, L.; Basolo, F.; Ferrannini, E.; Miccoli, P. Variable modulation by cytokines and thiazolidinediones of the prototype Th1 chemokine CXCL10 in anaplastic thyroid cancer. *Cytokine+* **2012**, *59* (2), 218−22.
(48) Shimazaki, N.; Togashi, N.; Hanai, M.; Isoyama, T.; Wada, K.; Fujita, T.; Fujiwara, K.; Kurakata, S. Anti-tumour activity of CS-7017, a selective peroxisome proliferator-activated receptor gamma agonist of thiazolidinedione class, in human tumour xenografts and a syngeneic tumour implant model. *Eur. J. Cancer* **2008**, *44* (12), 1734−43.
(49) Kang, D. W.; Choi, C. H.; Park, J. Y.; Kang, S. K.; Kim, Y. K. Ciglitazone induces caspase-independent apoptosis through down-regulation of XIAP and survivin in human glioma cells. *Neurochem. Res.* **2008**, *33* (3), 551−61.
(50) Dai, Y.; Qiao, L.; Chan, K. W.; Zou, B.; Ma, J.; Lan, H. Y.; Gu, Q.; Li, Z.; Wang, Y.; Wong, B. L.; Wong, B. C. Loss of XIAP sensitizes rosiglitazone-induced growth inhibition of colon cancer in vivo. *Int. J. Cancer* **2008**, *122* (12), 2858−63.
(51) Qiao, L.; Dai, Y.; Gu, Q.; Chan, K. W.; Zou, B.; Ma, J.; Wang, J.; Lan, H. Y.; Wong, B. C. Down-regulation of X-linked inhibitor of apoptosis synergistically enhanced peroxisome proliferator-activated receptor gamma ligand-induced growth inhibition in colon cancer. *Mol. Cancer Ther.* **2008**, *7* (7), 2203−11.
(52) Liu, J. J.; Guo, Y. W.; Fang, Z. G.; Si, X. N.; Wu, X. Y.; Liu, P. Q.; Lin, D. J.; Xiao, R. Z.; Xu, Y.; Wang, C. Z.; Li, X. D.; He, Y.; Huang, R. W. Activation of peroxisome proliferator-activated receptor-gamma induces apoptosis on acute promyelocytic leukemia cells via downregulation of XIAP. *Int. J. Mol. Med.* **2009**, *24* (5), 623−32.
(53) Zhao, X.; Xu, F.; Qi, B.; Hao, S.; Li, Y.; Li, Y.; Zou, L.; Lu, C.; Xu, G.; Hou, L. Serum metabolomics study of polycystic ovary syndrome based on liquid chromatography-mass spectrometry. *J. Proteome Res.* **2014**, *13* (2), 1101−11.
(54) Singh, V.; Chassaing, B.; Zhang, L.; San Yeoh, B.; Xiao, X.; Kumar, M.; Baker, M. T.; Cai, J.; Walker, R.; Borkowski, K.; Harvatine, K. J.; Singh, N.; Shearer, G. C.; Ntambi, J. M.; Joe, B.; Patterson, A. D.; Gewirtz, A. T.; Vijay-Kumar, M. Microbiota-Dependent Hepatic Lipogenesis Mediated by Stearoyl CoA Desaturase 1 (SCD1) Promotes Metabolic Syndrome in TLR5-Deficient Mice. *Cell Metab.* **2015**, *22* (6), 983−96.
(55) Bu, S. Y.; Mashek, M. T.; Mashek, D. G. Suppression of long chain acyl-CoA synthetase 3 decreases hepatic de novo fatty acid synthesis through decreased transcriptional activity. *J. Biol. Chem.* **2009**, *284* (44), 30474−83.
(56) Chen, W. C.; Wang, C. Y.; Hung, Y. H.; Weng, T. Y.; Yen, M. C.; Lai, M. D. Systematic Analysis of Gene Expression Alterations and Clinical Outcomes for Long-Chain Acyl-Coenzyme A Synthetase Family in Cancer. *PLoS One* **2016**, *11* (5), No. e0155660.
(57) Subramanian, A.; Miller, D. M. Structural analysis of alpha-enolase. Mapping the functional domains involved in down-regulation of the c-myc protooncogene. *J. Biol. Chem.* **2000**, *275* (8), 5958−65.
(58) Sugiura, K.; Pendola, F. L.; Eppig, J. J. Oocyte control of metabolic cooperativity between oocytes and companion granulosa cells: energy metabolism. *Dev. Biol.* **2005**, *279* (1), 20−30.
(59) Gillott, D. J.; Eldib, A.; Iammarrone, E.; Leung, K. Y.; Thornhill, A. R.; Grudzinskas, J. G. Glycolytic enzyme expression in human granulosa cells. *Fertil. Steril.* **2008**, *90* (4), 1405−10.
(60) Yoshioka, N.; Takahashi, N.; Tarumi, W.; Itoh, M. T.; Ishizuka, B. Gonadotropins up-regulate the expression of enolase 2, but not enolase 1, in the rat ovary. *Endocr. J.* **2011**, *58* (11), 941−8.
(61) Doolan, P.; Meleady, P.; Barron, N.; Henry, M.; Gallagher, R.; Gammell, P.; Melville, M.; Sinacore, M.; McCarthy, K.; Leonard, M.; Charlebois, T.; Clynes, M. Microarray and proteomics expression profiling identifies several candidates, including the valosin-containing protein (VCP), involved in regulating high cellular growth rate in production CHO cell lines. *Biotechnol. Bioeng.* **2010**, *106* (1), 42−56.

DOI: 10.1021/acs.jproteome.8b00917
J. Proteome Res. 2019, 18, 1691−1702